journal of the international meteor organization

WGN

50:6
december 2022

Long-term radio studies of
major and daytime meteor showers
High-inclination meteor showers
Meteor halo classification
Spectroscopy during the 2022 Perseids

ISSN 1016-3115

WGN Vol. 50, No. 6, December 2022, pp. 147 – 182

Administrative

Radio meteors

Ongoing meteor work

Front cover photo

Bright fireball captured during the Tau Herculid campaign on 2022 May 31 at $06^{\mathrm{h}}36^{\mathrm{m}}59^{\mathrm{s}}$ UT from Mt. Graham Observatory, Arizona, USA. DJI OSMO Action was employed with 2.7-mm $f/2.8$ lens and 25 s exposure at ISO 3200. Image courtesy: Stanislav Kaniansky.

Writing for WGN

This Journal welcomes papers submitted for publication. All papers are reviewed for scientific content, and edited for English and style. Instructions for authors can be found in WGN **45:1**, 1–5, and at `http://www.imo.net/docs/writingforwgn.pdf` .

Legal address

International Meteor Organization, Jozef Mattheessensstraat 60, 2540 Hove, Belgium.

Editorial — Call for papers

Javor Kac

Every journal's content depends on submissions from authors. We encourage you to write up your ideas and results for WGN. All kinds of meteor-related articles are welcome.

For instructions for authors, please see `https://www.imo.net/publications/wgn/` or refer to Kac (2017).

References

Kac J. (2017). "Writing for WGN". *WGN, Journal of the International Meteor Organization*, **45:1**, 1–5.

IMO bibcode WGN-506-editorial NASA-ADS bibcode 2022JIMO...50..147K

From the Treasurer — IMO Membership/WGN Subscription Renewal for 2023

Marc Gyssens

Renewal rates

Most members/subscribers whose membership/subscription has expired should have received a reminder email by the time you receive this issue of WGN. Via this way, we invite them again to renew for 2023.

The fees are as tabulated below. Notice that we have reduced the dollar rates to reflect the evolution of the exchange rate of the dollar versus the euro. We also continue to offer an electronic-only subscription at a reduced rate.

IMO Membership/WGN Subscription 2023				
Electronic + paper with surface mail delivery:		€26		US$ 30
Electronic + paper with airmail delivery (outside Europe only):		€49		US$ 56
Electronic only:		€21		US$ 24
Supporting membership:	add	€26	add	US$ 30

It is also possible to renew for two or more years in a row.

When you renew, give a few minutes of thought to becoming a **supporting member** by paying at least 26 EUR/30 USD extra. Smaller gifts are of course also appreciated. As you may know, there is an IMO Support Fund. With this Support Fund, we offer support to meteor-related projects. Our ability to provide this service to the meteor community depends primarily on the gifts we receive from supporting members!

Another way to help meteor workers with limited funds is to offer them a gift subscription.

We already thank all our members that will renew for their continued trust in our Organization!

Payment instructions

You first must log in into your account at the IMO website if you want to renew. For this purpose, click the log-in button in the upper right-hand corner. As login, use the email address on which you received my reminder email. In case you forgot your password, you can use the "forgot password" link to reset it. Once logged in, you will see your profile picture (or the space provided for it). If you read on the green button below it that your membership is about to expire, click it, and the rest will be self-explanatory.[1]

The outcome of this process is that you will see the total amount due and your payment options. If you choose to pay using PayPal (or using a credit card via PayPal), you can complete the payment on our website.

If you experience any difficulties, do not hesitate to contact me at `treasurer@imo.net`.

One final request: every year, a lot of members renew late. As a consequence, back issues that already appeared have to be sent out to these members. Please support our volunteers in their bimonthly effort to have WGN shipped to you by renewing promptly! Thank you for your understanding and cooperation!

IMO bibcode WGN-506-gyssens-renewal NASA-ADS bibcode 2022JIMO...50..147G

[1] Alternatively, you can also click on "Extend your membership" in the pull-down menu to the right of your name in the upper right-hand corner, with the same result.

Radio meteors

Long-Term Studies of Major and Daytime Meteor Showers using Worldwide Radio Meteor Observations

Hiroshi Ogawa[1]

Radio Meteor Observations are possible even during bad weather and during daytime. Using worldwide radio observations between 2001 and 2022 allows us to reconstruct meteor activity structures and annual variations. Our study is not restricted to major meteor showers but also includes daytime meteor showers.

Received 2022 November 27

1 Introduction

Continuous observations are very important when we discuss a study of a long-term analysis of meteor showers. On the other hand, however, optical observations are adversely affected by weather, daytime and human resources.

Radio Meteor Observation is a very useful method for meteor study because it is possible to observe even during bad weather or during daytime. Since radio meteor observing using forward-scatter is very easy, a lot of observing stations are working in the world. Besides, it becomes possible to monitor a complete meteor activity profile without influence of radiant elevation by using worldwide data.

The International Project for Radio Meteor Observations (IPRMO) was set up in 2001. Its purpose was the observation of the complete Leonid meteor shower. As a result, it succeeded to reconstruct the global shower activity of the Leonids 2001 (Ogawa et al., 2002). After the Leonids, IPRMO has continued to collect data of worldwide radio meteor observations. Collected data pointed out activity structures of major meteor showers including daytime meteor showers (Ogawa & Steyaert, 2017).

The present study is not only an analysis of the activity structure of meteor showers but also of the annual variation through a long-term monitoring of major and daytime meteor showers using worldwide radio meteor observations.

2 Method

2.1 Activity Level Index

2.1.1 Motivation

When worldwide data are integrated, a correction factor is needed just like for visual observations. Although for visual observations a way has been determined to correct the observed data to a Zenithal Hourly Rate by using limiting magnitude and amount of clouds, this has not been done for radio meteor observations yet. There are a lot of factors to consider such as location, radio frequency, antenna, receiver, cable, software and the counting system of meteor echoes (manual or automatic). It is therefore difficult to integrate worldwide data and to convert them to Zenithal Hourly Rate.

2.1.2 Definition

As a solution, an index for estimating meteor activity was adopted. It is named "Activity Level" (Ogawa et al., 2001) and is defined by the following formula.

$$A(t) = \frac{1}{N}\sum_{i=1}^{N}\left(\frac{H_{\mathrm{obs}_i}(t) - H_{\mathrm{spo}_i}(T)}{D_{\mathrm{spo}_i}} \times \frac{1}{\sin h_i(t)}\right)$$

where N is the number of observing stations, H_{obs} the hourly number of observed meteor echoes at station i at time t, H_{spo} the background hourly rate at station i at hour of the day t, D_{spo} the background average for a day ($D_{\mathrm{spo},i} = \frac{1}{24}\sum_{T=0}^{23} H_{\mathrm{spo},i}(T)$), and $h(t)$ the radiant elevation at station i at time t. A detailed explanation can be found in the Handbook for Meteor Observers (Rendtel, 2022).

2.1.3 Characteristics

The Activity Level Index has already been used in some previous studies. Although it is useful to integrate worldwide data, it has a few caveats.

One is related to periods of no-meteor shower activity. In periods without meteor shower activity, the Activity Level Index was 0.01 ± 0.29 (using February, March and September in the period of 2002–2021). If the activity level is within ± 0.3, therefore, chances are that this is just background activity.

A second caveat is that it is impossible to compare activity levels and profiles of different meteor showers. This is because the Activity Level Index does not only depend on meteor influx but also on geocentric velocity and population index of the meteor shower and on the forward scatter frequency.

2.2 Estimated activity structures

Activity profiles were estimated based on Lorentz Profiles (Jenniskens et al., 2000), with a least squares method. In this way, it became possible to estimate peak longitudes, maximum activity levels, and durations of ascending and descending branches.

2.3 Annual variations

Long-term studies provide insight into the annual variation of meteor activity. In this study three patterns

[1]The International Project for Radio Meteor Observations (IPRMO), Midorino 2-14-3, Tsukuba, Ibaraki, 305-0881, Japan. Email: h-ogawa@iprmo.org

IMO bibcode WGN-506-ogawa-radio
NASA-ADS bibcode 2022JIMO...50..148O

were calculated: "Past average", "10 years average" and "5 years average".

"Past average" is calculated by all data before the considered time. When the "past average" of 2022 is calculated, all data before 2022 are used.

The "10 years average" is the average for the preceding period of 10 years. For example, the "10 years average of 2019" is calculated using all data of the period 2010–2019.

The "5 years average" is the average for the preceding period of 5 years. For example, the "5 years average of 2015" is calculated using all data for the period of 2011–2015.

3 Data

Observed data were provided by Radio Meteor Observation Bulletin (RMOB)[a] and Radio Meteor Observations in Japan (RMOJ)[b]. The data were collected at more than 50 observing sites in more than 15 countries.

4 Results and Discussion

4.1 Quadrantids (010 QUA)

4.1.1 Estimated Activity Structure

The Quadrantids are one of the major meteor showers and are known for their narrow peak and high activity in visual observations. The activity profile of the Quadrantids was calculated using the Activity Level Index and covers the period 2001–2022 (Figure 1).

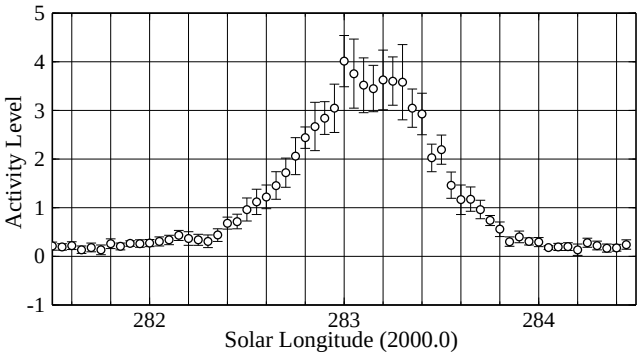

Figure 1 – The activity profile of the Quadrantids for every 0.°05 in solar longitude, calculated using the Activity Level Index, and covering the period 2001–2022.

The beginning of meteor activity was around $\lambda_\odot = 282.°4$, the peak occurred at $\lambda_\odot = 283.°15$ and the end was around $\lambda_\odot = 284.°0$. The maximum Activity Level was 4.0 and Full Width at Half Maximum (FWHM) is $-0.°4/+0.°3$.

4.1.2 Annual Variation

Figure 2 shows the annual variation of the Quadrantids. Maximum Activity Level and duration of the ascending and descending branch have not changed much in the past average and ten years average.

Although the past average has a fairly flat curve, the variations in 5- and 10-years average of the peak

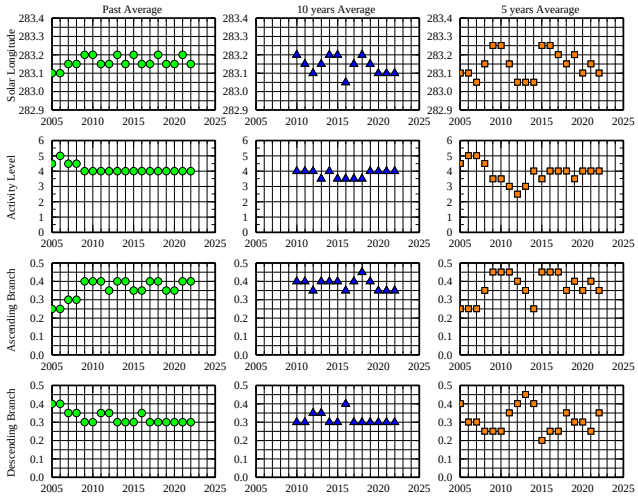

Figure 2 – The annual variation of the Quadrantids (Top row: peak solar longitude, 2nd row: maximum Activity Level, 3rd row: duration of ascending branch, and bottom row: duration of descending branch. Left column: past average, middle column: 10 years average and right column: 5 years average.).

solar longitude are much more pronounced. The peak solar longitude for the period 2009–2010 was around $\lambda_\odot = 283.°25$ in the five years average. Then, the period 2012–2014 shows an earlier peak around $\lambda_\odot = 283.°05$. During the period 2015–2016, it came later, again around $\lambda_\odot = 283.°25$. After that, the peak solar longitude fell earlier again.

4.1.3 Discussion

Although the peak time was estimated at $\lambda_\odot = 283.°15$, there is a high activity level during the entire period of $\lambda_\odot = 283.°0 - 283.°3$. Possible interpretations are that a peak structure kept high activity, a change of peak time occurred for this period, or the apparent flat peak was caused by an influence of the "zenithal effect".

A previous study described that the peak time during the period 2011–2016 was earlier than during the period 2001–2010 (Ogawa & Steyaert, 2017). The 10 years average of 2010 and 2016 in Figure 2 shows the same result. Moreover, as described in Section 4.1.2, the 5 years average shows a peak solar longitude at $\lambda_\odot = 283.°05$ during the period 2012–2014, and at $\lambda_\odot = 283.°25$ during the periods 2009–1010 and 2015–2019. Possibly, the "flat peak" is caused by the variation in the peak solar longitude.

Another possible interpretation, a zenithal effect, was also described in previous research. The zenithal effect is a temporary decrease in the Activity Level when the radiant is located around the zenith. The "flat peak" was caused by a temporary decrease around $\lambda_\odot = 283.°2$. Therefore, possibly the real activity level around that time was much higher than calculated. However, observational data corresponding to high radiant elevations ($h > 70°$) were removed in the process of calculating the Activity Level Index. Nevertheless, it cannot be excluded that the zenithal effect occurred at lower radiant elevation in some cases. This depends on the distance between the transmitting and receiving stations, the radio frequency and the latitude of the observing station.

[a] https://www.rmob.org
[b] https://www.iprmo.org

4.2 April Lyrids (006 LYR)

4.2.1 Estimated Activity Structure

The April Lyrids show a clear annual activity although there are not many visual observations during that time of the year. A long-term study also revealed the complete meteor activity profile (Figure 3).

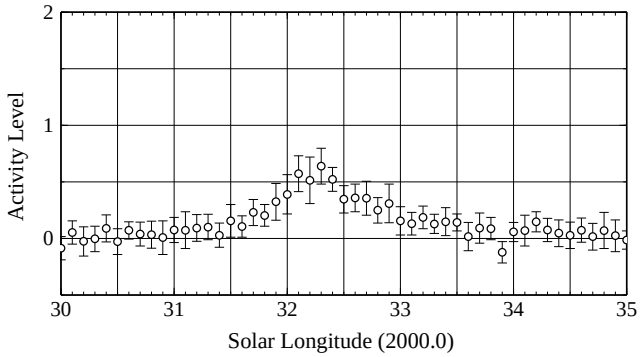

Figure 3 – The activity profile of the April Lyrids in steps of $0\overset{\circ}{.}1$ in solar longitude, calculated using the Activity Level Index, and covering the period 2001–2022.

A clear activity started at $\lambda_\odot = 31\overset{\circ}{.}6$. The activity level was climbing, the peak came at $\lambda_\odot = 32\overset{\circ}{.}2$ with Activity Level = 0.6. According to the IMO Meteor Shower Calendar, the peak time occurs at $\lambda_\odot = 32\overset{\circ}{.}32$ (Rendtel, 2021). The peak time therefore was a little early. After the peak, April Lyrids activity ends around $\lambda_\odot = 33\overset{\circ}{.}6$. The FWHM was $-0\overset{\circ}{.}4/+0\overset{\circ}{.}6$. A past research about FWHM described that it was between $1\overset{\circ}{.}1$ to $1\overset{\circ}{.}4$ (Dubietis & Arlt, 2001). Since 2007, there was no unusual or outburst activity.

4.2.2 Annual Variation

Figure 4 shows the annual variation of the April Lyrids.

Although the past average of the peak solar longitude has a fairly flat curve, the peak solar longitude falls later and later in the five- and ten-years average. If this trend continues, the past average should evolve in the same way.

4.3 η-Aquariids (031 ETA)

4.3.1 Estimated Activity Structure

The η-Aquariids, released from 1P/Halley, produce the activity profile shown in Figure 5. A clear activity started around $\lambda_\odot = 41\overset{\circ}{.}5$. After the main peak around $\lambda_\odot = 44\overset{\circ}{.}0 - 46\overset{\circ}{.}0$, the activity level becomes weaker and weaker.

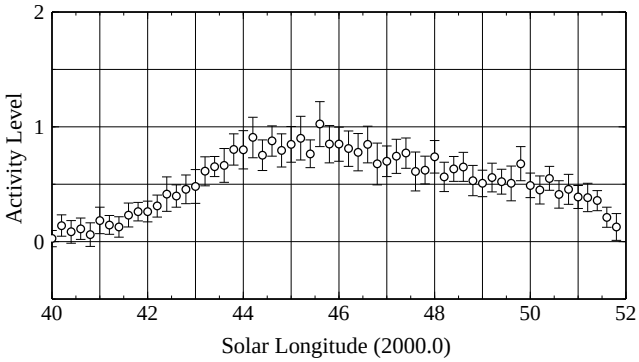

Figure 5 – The activity profile of the η-Aquariids in steps of $0\overset{\circ}{.}2$ in solar longitude, calculated using the Activity Level Index, and covering the period 2004–2022.

The peak occurred at $\lambda_\odot = 44\overset{\circ}{.}3$ with Activity Level = 0.8. Although the peak time was a day earlier than that of visual observations at $\lambda_\odot = 45\overset{\circ}{.}5$ (Rendtel, 2022), a high activity continued for the period $\lambda_\odot = 44\overset{\circ}{.}0 - 46\overset{\circ}{.}0$. The FWHM was $1\overset{\circ}{.}6/+7\overset{\circ}{.}2$. The descending branch took much longer than the ascending branch.

4.3.2 Annual Variation

Figure 6 shows the annual variation of the η-Aquariids.

A big change around 2012 was caused by high activities around 2012–2013. An outburst was observed by

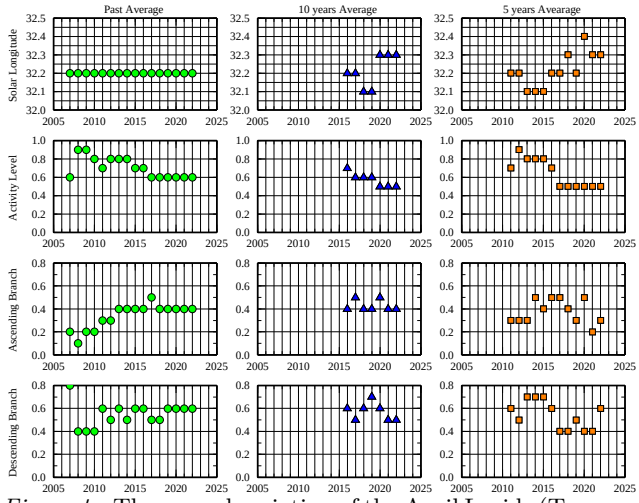

Figure 4 – The annual variation of the April Lyrids (Top row: peak solar longitude, 2nd row: maximum Activity Level, 3rd row: duration of ascending branch, and bottom row: duration of descending branch. Left column: past average, middle column: 10 years average and right column: 5 years average.).

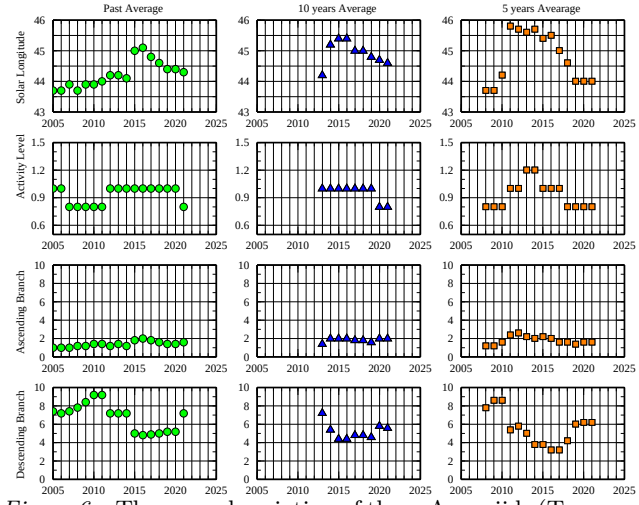

Figure 6 – The annual variation of the η-Aquariids (Top row: peak solar longitude, 2nd row: maximum Activity Level, 3rd row: duration of ascending branch, and bottom row: duration of descending branch. Left column: past average, middle column: 10 years average and right column: 5 years average.).

optical observations (Johannink, 2013) and radio observations (Steyaert, 2014) in 2013. The activity level was also higher than the average level in 2012. As a result, the peak time was later and the corresponding Activity Level was higher.

4.3.3 Discussion

Although the descending branch took much longer than the ascending branch (Figure 5), it is possible that it was artificially prolonged by the contribution of other daytime meteor showers such as the Northern ω-Cetids ($\alpha = 9°$, $\delta = +11°$) at $\lambda_\odot = 47\overset{\circ}{.}5$, the Southern ω-Cetids ($\alpha = 23°$, $\delta = -3°$) at $\lambda_\odot = 49\overset{\circ}{.}5$ or the ε-Arietids ($\alpha = 44°$, $\delta = +21°$) at $\lambda_\odot = 48\overset{\circ}{.}7$.

The activity profile was fit to the sum of two Lorentz profiles, which yielded 2 components (Figure 7). One component corresponds to the main η-Aquariid activity which had a maximum Activity Level of 0.8 at $\lambda_\odot = 45\overset{\circ}{.}3$ with FWHM $= -2\overset{\circ}{.}5/+2\overset{\circ}{.}5$ (Comp 1 in Figure 7). The peak time was near that of visual observations (at $\lambda_\odot = 45\overset{\circ}{.}5$) in this case. Moreover, video observations published by SonotaCo Net 2007–2018 (Koseki, 2021) show a similar result (at $\lambda_\odot = 45\overset{\circ}{.}0$). The other component had a maximum Activity Level of 0.3 at $\lambda_\odot = 49\overset{\circ}{.}2$ with FWHM $= -2\overset{\circ}{.}5/+3\overset{\circ}{.}5$ (Comp 2). Possibly this component was caused by other daytime meteor showers. It was possible to separate the activity into two components every year (Table 1).

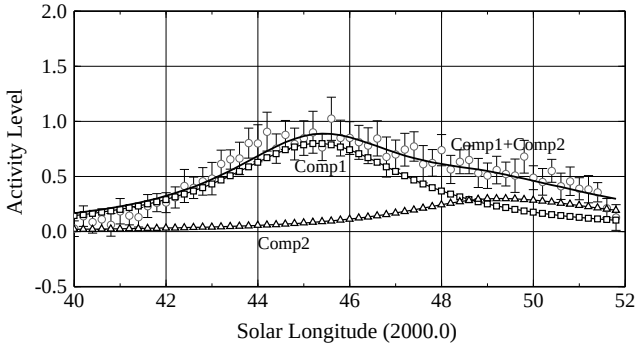

Figure 7 – An activity profile of the η-Aquariids separated into 2 components. (The curve with squares refers to Component 1 (main η-Aquariid activity), the curve with triangles refers to Component 2, the solid line refers to the total of Components 1 and 2, and the circles with error bars show the activity level of η-Aquariids.)

4.4 Southern δ-Aquariids (005 SDA)

4.4.1 Estimated Activity Structure

The Southern δ-Aquariids show a lot of activity at the end of July in radio meteor observations although they are less prominent in visual observations. Figure 8 shows an estimated activity profile.

Southern δ-Aquariid activity started around $\lambda_\odot = 117°$, and the peak had an Activity Level of 3.0 at $\lambda_\odot = 124\overset{\circ}{.}8$ with FWHM $= -3.0/+5.5$. The descending branch took longer than the ascending branch. After the peak time, the Activity Level became weaker and weaker.

Table 1 – Estimated Components of η-Aquariid activity

	Comp-1		Comp-2	
Year	$\lambda_{\odot\max}$	$A_{\max}$	$\lambda_{\odot\max}$	$A_{\max}$
2022	$45\overset{\circ}{.}27$	1.0	$50\overset{\circ}{.}06$	0.4
2021	$45\overset{\circ}{.}15$	0.7	$48\overset{\circ}{.}73$	0.3
2020	$45\overset{\circ}{.}52$	1.1	$50\overset{\circ}{.}15$	0.5
2019	$44\overset{\circ}{.}60$	1.0	$49\overset{\circ}{.}32$	0.5
2018	$44\overset{\circ}{.}76$	1.5	$48\overset{\circ}{.}99$	0.5
2017	$45\overset{\circ}{.}41$	1.3	$49\overset{\circ}{.}44$	0.5
2016	$45\overset{\circ}{.}70$	1.0	$49\overset{\circ}{.}53$	1.0
2015	$43\overset{\circ}{.}77$	1.5	$49\overset{\circ}{.}77$	0.5
2014	$45\overset{\circ}{.}23$	1.0	$49\overset{\circ}{.}10$	0.5
2013	$45\overset{\circ}{.}47$	3.0	—	—
2012	$45\overset{\circ}{.}72$	2.0	$50\overset{\circ}{.}52$	0.5
2011	$45\overset{\circ}{.}98$	1.3	$48\overset{\circ}{.}96$	0.5
2010	$46\overset{\circ}{.}22$	1.3	$50\overset{\circ}{.}57$	0.6
2009	$44\overset{\circ}{.}05$	0.6	$47\overset{\circ}{.}08$	1.2
2008	$45\overset{\circ}{.}51$	1.3	$49\overset{\circ}{.}14$	0.7
2007	$45\overset{\circ}{.}96$	1.0	$48\overset{\circ}{.}42$	0.5
2006	$45\overset{\circ}{.}77$	0.8	$50\overset{\circ}{.}12$	0.5
2005	$46\overset{\circ}{.}45$	1.5	$50\overset{\circ}{.}36$	0.5
2004	$44\overset{\circ}{.}81$	1.5	$49\overset{\circ}{.}84$	0.5

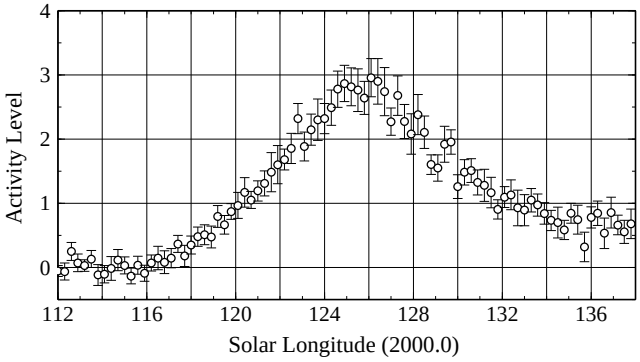

Figure 8 – The activity profile of the Southern δ-Aquariids in steps of $0\overset{\circ}{.}3$ in solar longitude, calculated using the Activity Level Index, and covering the period 2005–2022.

4.4.2 Annual Variation

The annual variation of Southern δ-Aquariids is shown in Figure 9. The peak solar longitude fell earlier year after year in the graph of the past average. A clear decrease in the Activity Level and increase in the duration of the descending branch was seen in the five years average. Although a big change was seen between 2013 and 2014 in the five years average, the reason for this change is not clear yet.

4.4.3 Discussion

For the Southern δ-Aquariids, there are three interesting discussion points. They concern the peak time, the wide descending branch and the high activity.

The first discussion point is that the estimated peak time of radio meteor observations ($\lambda_\odot = 124\overset{\circ}{.}8$) was much earlier than that of visual ($\lambda_\odot = 127°$ according to Rendtel, 2022) and video ($\lambda_\odot = 127\overset{\circ}{.}6$ according to Koseki, 2021) observations. Possibly, this discrepancy was caused by differences of observable magnitude between radio and optical observations. Although it

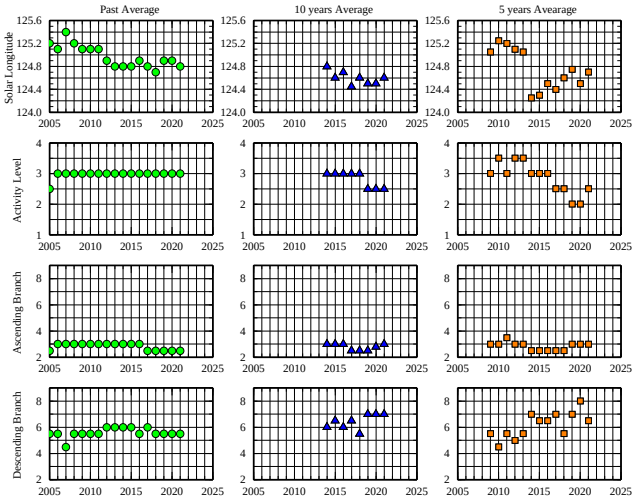

Figure 9 – The annual variation of the Southern δ-Aquariids (Top row: peak solar longitude, 2nd row: maximum Activity Level, 3rd row: duration of ascending branch, and bottom row: duration of descending branch. Left column: past average, middle column: 10 years average and right column: 5 years average.).

depends on the geocentric velocity, radio meteor observations allow detection of fainter meteors compared to visual observations. For example, a frequency around 50 MHz allows detection of sixth magnitude meteors in the case of underdense echoes (Miyao & Ogawa, 2004).

The second point is that the descending branch took longer than the ascending branch. Possibly, this was caused by other meteor shower activity than that of the Southern δ-Aquariids. The Perseids and α-Capricornids show activity from the end of July onward into August. Since the α-Capricornids do not show strong activity, it seems that the influence was due to the beginning activity of the Perseids.

The third interesting point is that this shower shows higher Activity Levels than other meteor showers in radio meteor observations. The Activity Level of the Southern δ-Aquariids in visual observations reaches ZHR = 25 (Rendtel, 2022). In comparison, the Perseids have a maximum ZHR around 100. The maximum Activity Level Southern δ-Aquariids in radio meteor observation is comparable to that of the Quadrantids and the Geminids. It seems that this discrepancy is caused by a combination of geocentric velocity, forward scatter frequency and population index (McKinley, 1961), but it is not clear which factor is the strongest. The Southern δ-Aquariids have $V_\infty = 41$ km/s and $r = 2.5$. Possibly these parameters result in good conditions for radio meteor observations.

4.5 Perseids (007 PER)

4.5.1 Estimated Activity Structure

Although the Perseids are one of the most excellent meteor showers in visual observations, they do not show high activity in radio meteor observations, probably because of a combination of fast geocentric velocity and low population index. Figure 10 shows the estimated activity profile covering the period 2001–2022.

A peak occurred at $\lambda_\odot = 140\overset{\circ}{.}0$ with Activity Level of 1.2 and FWHM $= -0\overset{\circ}{.}70/+0\overset{\circ}{.}75$. High activity continued during the period $\lambda_\odot = 139\overset{\circ}{.}7 - 140\overset{\circ}{.}1$. Clearly

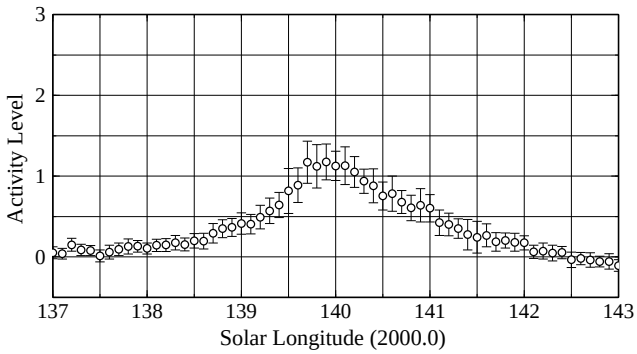

Figure 10 – The activity profile of the Perseids in steps of $0\overset{\circ}{.}1$ in solar longitude, calculated using the Activity Level Index, and covering the period 2001–2022.

discernible activity started at $\lambda_\odot = 138\overset{\circ}{.}5$. After the peak was over, activity faded at $\lambda_\odot = 142\overset{\circ}{.}0$. The descending branch lasted a little longer than the ascending branch.

4.5.2 Annual Variation

Figure 11 shows the annual variation of the Perseids.

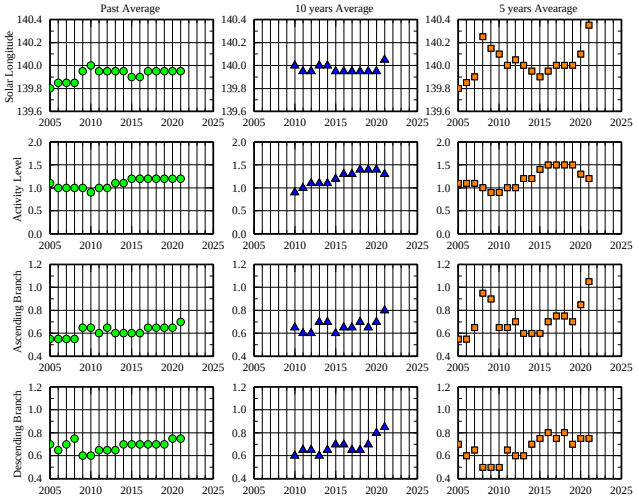

Figure 11 – The annual variation of the Perseids (Top row: peak solar longitude, 2nd row: maximum Activity Level, 3rd row: duration of ascending branch, and bottom row: duration of descending branch. Left column: past average, middle column: 10 years average and right column: 5 years average.).

The later peak in recent years was caused by an unexpected peak around $\lambda_\odot = 141\overset{\circ}{.}5$. A surprise peak was observed at $\lambda_\odot = 141\overset{\circ}{.}5$ in 2021 (Miskotte et al., 2021). In other years, a small sub-peak around $\lambda_\odot = 141\overset{\circ}{.}5$ was also observed. Besides, a change in 2008 was caused by high activity in 2008 and 2009 (Jenniskens et al., 2008; Jenniskens et al., 2008).

4.5.3 Discussion

Figure 10 shows that the descending branch is longer than the ascending branch. Figure 11 shows the descending branch lasted longer year after year. Although this was caused by an unpredicted peak around $\lambda_\odot = 141\overset{\circ}{.}5$, it seems that the peak time shifted to later values recently. Table 2 shows the estimated traditional peak time since 2009 (not including unexpected and predicted outburst activity). It shows that peaks during for the period of 2018–2022 occurred between $\lambda_\odot =$

Table 2 – Estimated traditional peak of Perseids.

Year	$\lambda_\odot$	Year	$\lambda_\odot$
2022	140.°29	2015	139.°80
2021	140.°53	2014	139.°93
2020	140.°17	2013	139.°94
2019	140.°10	2012	139.°90
2018	140.°11	2011	139.°87
2017	139.°91	2010	140.°00
2016	139.°75	2009	139.°88

140.°1 and $\lambda_\odot = 140.°5$. On the other hand, maximum activity before 2017 occurred between $\lambda_\odot = 139.°7$ and $\lambda_\odot = 140.°0$.

4.6 Orionids (008 ORI)

4.6.1 Estimated Activity Structure

The Orionids in radio meteor observations do not show a high activity, just like the Perseids. This is probably due to a combination of the high geocentric velocity and the rather low population index. Figure 12 shows the activity profile of the Orionids covering the period 2004–2021.

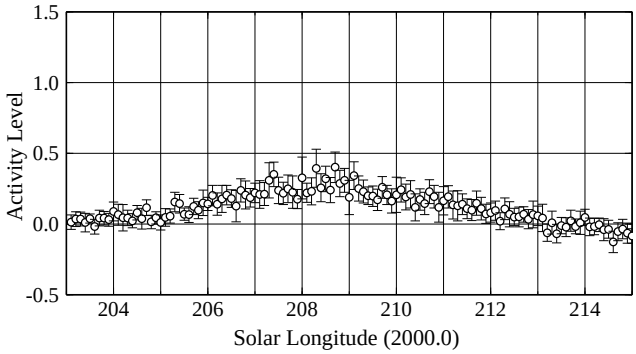

Figure 12 – The activity profile of the Orionids in steps of 0.°1 in solar longitude, calculated using the Activity Level Index, and covering the period 2004–2021.

The peak was estimated at $\lambda_\odot = 208.°6$ with a maximum Activity Level of 0.3 and FWHM $= -2.°3/+1.°8$. Clear activity started at $\lambda_\odot = 205.°5$, and ended around $\lambda_\odot = 213°$.

4.6.2 Annual Variation

Figure 13 shows the annual variation of the Orionids. The Orionids showed a high activity in 2006 and 2007 (Arlt et al., 2008). The Activity Level became weaker and weaker after this event.

Since the activity level became weaker, it became difficult to estimate the peak time, and the duration of the ascending and descending branches. In the five-years average, therefore, estimated values were unstable in recent years.

4.7 Geminids (004 GEM)

4.7.1 Estimated Activity Structure

The Geminids are one of the most excellent meteor showers. Radio meteor observations allow to observe a lot of Geminid echoes. Figure 14 shows the activity

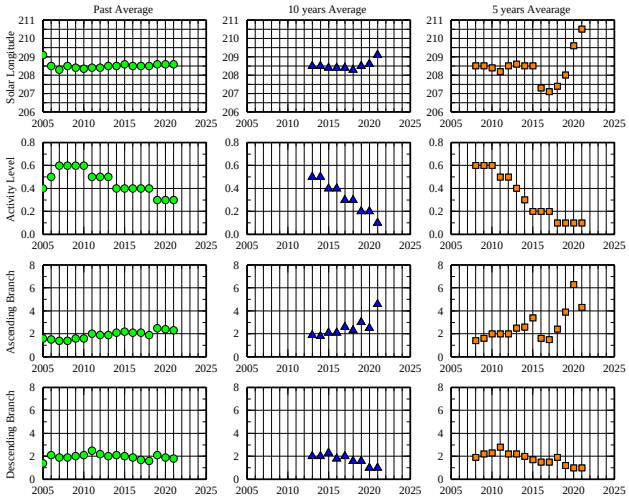

Figure 13 – The annual variation of the Orionids (Top row: peak solar longitude, 2nd row: maximum Activity Level, 3rd row: duration of ascending branch, and bottom row: duration of descending branch. Left column: past average, middle column: 10 years average and right column: 5 years average.).

profile of the Geminids for the period 2002–2021. Noticeable activity started around $\lambda_\odot = 256°$, the peak occurred at $\lambda_\odot = 261.°95$, and the activity ended at $\lambda_\odot = 263.°5$. The ascending branch (FWHM of 1.°30) was much wider than the descending branch (FWHM of 0.°50).

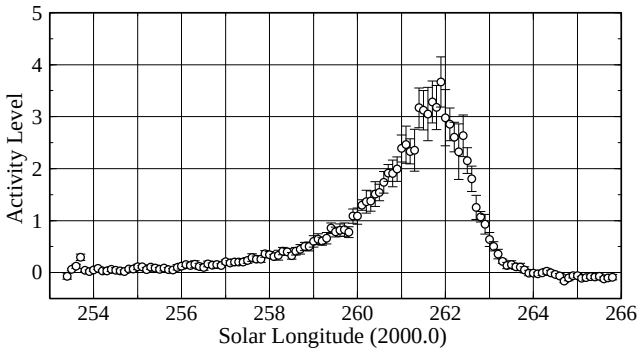

Figure 14 – The activity profile of the Geminids in steps of 0.°1 in solar longitude, calculated using the Activity Level Index, and covering the period 2002–2021.

4.7.2 Annual Variation

Figure 15 shows the annual variation of the Geminids. The activity level increased year after year.

4.8 Discussion

There are two discussion points concerning the Geminids. One is the continuous high activity. The other is a difference in peak time between radio and visual observations.

Concerning the first point, Figure 14 shows that there is a high activity during the period $\lambda_\odot = 261.°4 - 262.°1$. Ogawa and Steyaert (2017) described that the peak time for the period of 2011–2016 was later than the period of 2002–2010. Possibly some early peak time in the '00s led to the flat peak structure.

We now turn to the second point. Although a peak time in this study was estimated at $\lambda_\odot = 261.°95$,

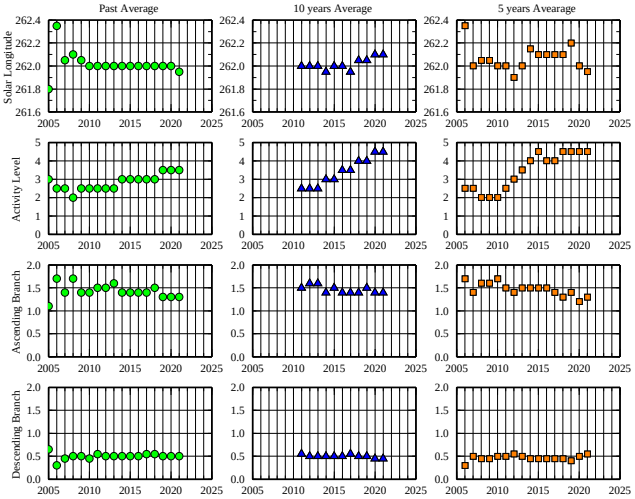

Figure 15 – The annual variation of the Geminids (Top row: peak solar longitude, 2nd row: maximum Activity Level, 3rd row: duration of ascending branch, and bottom row: duration of descending branch. Left column: past average, middle column: 10 years average and right column: 5 years average.).

visual observations caught it at $\lambda_{\odot} = 262\,^{\circ}2$ (Rendtel, 2022). Since in radio observations it is possible to observe fainter meteors compared to visual observations, it seems that, in the case of the Geminids, a difference in detectable meteors led to a difference in peak time. This it might be caused by the Poynting-Robertson effect. Uchiyama (2010) researched the difference in peak time for each magnitude class using visual observations. It was concluded that the peak time for brighter magnitude is later than for fainter meteors: $T_{\max}(m) = 262\,^{\circ}328 - 0\,^{\circ}055M$, where m is meteor magnitude and $T_{\max}(m)$ solar longitude of the peak for magnitude m.). This seems a plausible explanation for the different peak times in radio and visual observations.

4.9 Ursids (015 URS)

4.9.1 Estimated Activity Structure

Figure 16 shows the estimated activity profile of the Ursids. The beginning of Ursid activity was around $\lambda_{\odot} = 269\,^{\circ}4$, the peak occurred at $\lambda_{\odot} = 270\,^{\circ}6$. The FWHM was between $-0\,^{\circ}55$ and $+0\,^{\circ}35$ and the maximum Activity Level was around 0.4. After the peak, activity ended at $\lambda_{\odot} = 271\,^{\circ}6$. Although it was not high, clear activity was observed every year.

4.9.2 Annual Variation

Figure 17 shows the annual variation of the Ursids. A big change of trend was seen around 2015–2016. This was caused by encountering the 1392 dust trail in 2014 (Brown et al., 2015) as a consequence of which a higher activity was observed at $\lambda_{\odot} = 270\,^{\circ}77$ in 2016 (Rendtel et al., 2017). Moreover, IPRMO detected a higher activity in 2017 at twice the usual level before 2017.

4.10 Daytime April Piscids (144 APS)

4.10.1 Estimated Activity Structure

The Daytime April Piscids show a low activity during the same period as the April Lyrids. There were

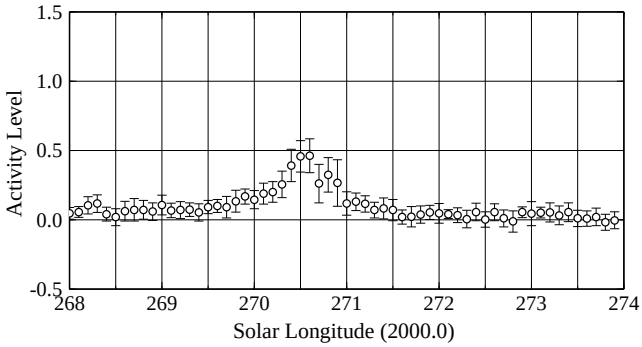

Figure 16 – The activity profile of the Ursids in steps of $0\,^{\circ}1$ in solar longitude, calculated using the Activity Level Index, and covering the period 2004–2021.

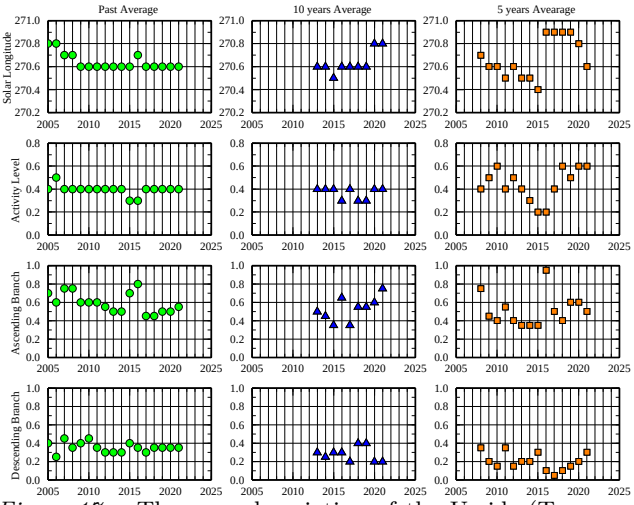

Figure 17 – The annual variation of the Ursids (Top row: peak solar longitude, 2nd row: maximum Activity Level, 3rd row: duration of ascending branch, and bottom row: duration of descending branch. Left column: past average, middle column: 10 years average and right column: 5 years average.).

a few studies about Daytime April Piscids. The maximum Activity Level was around 0.5 at $\lambda_{\odot} = 32\,^{\circ}6$, with FWHM $= -2\,^{\circ}4$ / $+2\,^{\circ}0$ (Figure 18). The peak time was in line with the latest IMO Calendar, which gives $\lambda_{\odot\max} = 32\,^{\circ}5$ (Rendtel, 2021). It started to appear around $\lambda_{\odot} = 30\,^{\circ}5$. After the maximum, discernable activity was over around $\lambda_{\odot} = 34\,^{\circ}5$. The Activity Level stayed elevated after the end of the activity period, but this was possibly due to other meteor showers such as the beginning of the η-Aquariid activity.

4.10.2 Annual Variation

Figure 19 shows the annual variation of the Daytime April Piscids. There was an unusual change in the five years average around 2017–2019; the peak solar longitude became later and the ascending and descending branches lasted shorter in the graphs of the 10 year average. This may be due to errors.

4.10.3 Discussion

There were a few studies about the Daytime April Pisids. Although the peak time in this study was later than in the Meteor Shower Workbook 2014 (Rendtel, 2014) which gives $\lambda_{\odot\max} = 30\,^{\circ}3$, the latest IMO Calen-

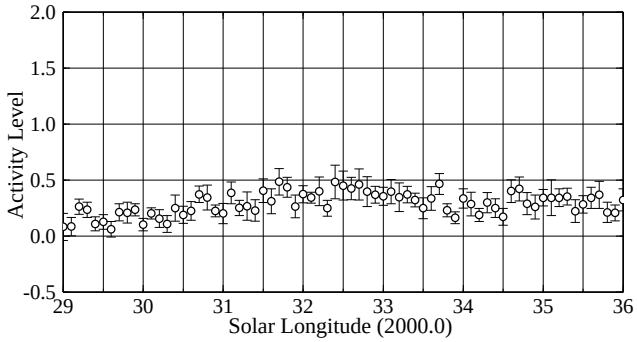

Figure 18 – The activity profile of the Daytime April Piscids in steps of 0.°1 in solar longitude, calculated using the Activity Level Index, and covering the period 2007–2022.

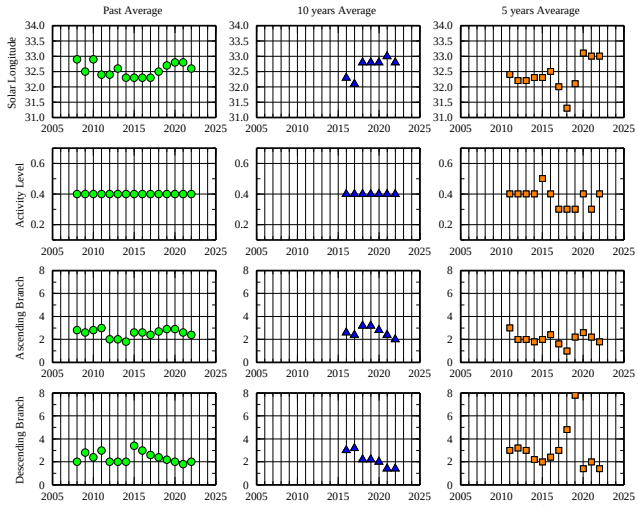

Figure 19 – The annual variation of the Daytime April Piscids (Top row: peak solar longitude, 2nd row: maximum Activity Level, 3rd row: duration of ascending branch, and bottom row: duration of descending branch. Left column: past average, middle column: 10 years average and right column: 5 years average.).

dar indicated a similar value, $\lambda_{\odot\max} = 32.°5$ (Rendtel, 2021).

4.11 Daytime Arietids (171 ARI)

4.11.1 Estimated Activity Structure

The Daytime Arietids, which are the biggest daytime meteor shower, show a high activity in June. Figure 20 exhibits the estimated activity profile during the period 2006–2022. Clear activity started around $\lambda_\odot = 73.°0$ and the end was around $\lambda_\odot = 88.°04$.

The Daytime ζ-Perseids have their peak at the same time. Figure 21 shows the estimated activity separated into 2 components.

One component corresponds to the Daytime Arietids (Comp1), and the other one corresponds to the influence of the other meteor shower (Comp2). The component of the Daytime Arietids (Comp1) had a peak at $\lambda_\odot = 77.°8$ with Activity Level 1.0. The FWHM was estimated as $-5.°5$ / $+5.°1$.

4.11.2 Annual Variation

Figure 22 shows the annual variation of the Daytime Arietids component (Comp1). The activity level became weaker and weaker in the five years average.

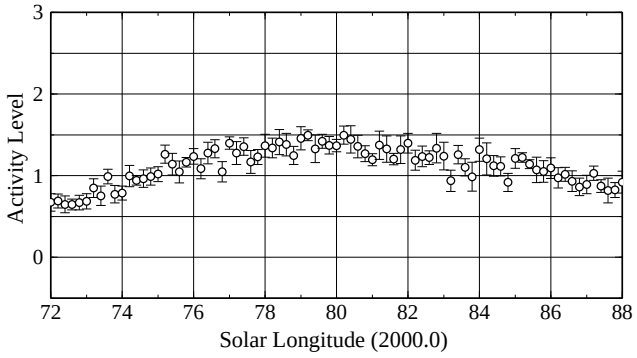

Figure 20 – The activity profile of the Daytime Arietids in steps of 0.°2 in solar longitude, calculated using the Activity Level Index, and covering the period 2006–2022.

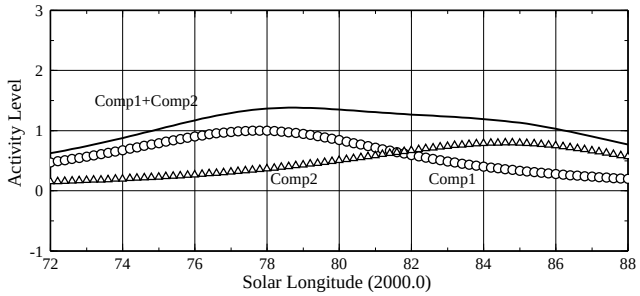

Figure 21 – Estimated components (circles refer to Comp1, triangles to Comp2 and the solid line to their sum.

4.11.3 Discussion

The estimated peak solar longitude in this study ($\lambda_\odot = 77.°8$) was later than the value published by the IMO. According to the Meteor Shower Workbook 2022 (Rendtel, 2022), the peak occurs at $\lambda_\odot = 76.°6$. SonotaCo Net video observations recorded the peak at $\lambda_\odot = 77°$ (Koseki, 2021). Since it is very difficult to estimate Daytime Arietid activity using forward-scatter observations, we need to continue to observe and analyze them in the future.

4.12 Daytime ζ-Perseids (172 ZPE)

The Daytime ζ-Perseids are active around the same time as the Daytime Arietids. Figure 23 shows an estimated activity profile using parameters of the ζ-Perseids.

This activity profile in Figure 23 could be separated into 2 components (Figure 24). Comp1 has a peak Activity Level of 0.9 with FWHM = $-8.°0$ / $+6.°0$ at $\lambda_\odot = 78.°4$. Comp2 has a peak Activity Level of 0.7 with FWHM = $-5.°0$ / $+7.°5$ at $\lambda_\odot = 83.°5$. It is very difficult to say which one was the Daytime ζ-Perseids (see Discussion).

4.12.1 Discussion

There are some references for the peak solar longitude of ζ-Perseids. For example, the latest IMO shower calendar (Rendtel, 2021) has put the peak at $\lambda_\odot = 78.°6$. This value corresponds to the peak of Comp1 ($\lambda_\odot = 78.°4$). However, the Daytime meteor working list in the past Meteor Shower Workbook 2014 (Rendtel, 2014) put the peak at $\lambda_\odot = 83.°5$. Therefore, it is

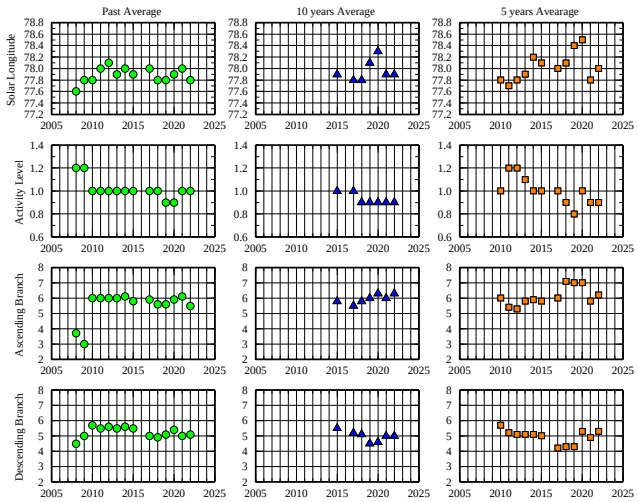

Figure 22 – The annual variation of the Daytime Arietids (Top row: peak solar longitude, 2nd row: maximum Activity Level, 3rd row: duration of ascending branch, and bottom row: duration of descending branch. Left column: past average, middle column: 10 years average and right column: 5 years average.).

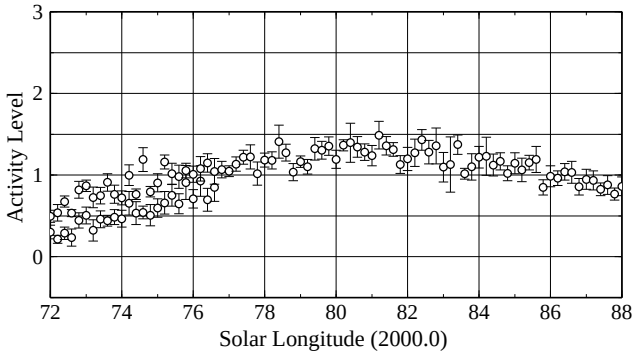

Figure 23 – The activity profile of the Daytime ζ-Perseids in steps of 0.°2 in solar longitude, calculated using the Activity Level Index, and covering the period 2006–2022.

possible that Comp2 ($\lambda_\odot = 83.°5$) corresponds to the ζ-Perseid activity. We need to further discuss the activity structure of the ζ-Perseids.

4.13 Daytime Sextantids (221 DSX)

4.13.1 Estimated Activity Structure

At the end of September, the Daytime Sextantids show some minor activity. Figure 25 exhibits the estimated activity profile of the Daytime Sextantids.

The activity began around $\lambda_\odot = 185°$. The peak occurred at $\lambda_\odot = 188.°8$ with FWHM $= -2.°4$ / $+2.°6$. The maximum activity level was estimated as 0.3. After the peak time, the eactivity ended around $\lambda_\odot = 192°$.

4.13.2 Annual Variation

Figure 26 shows the annual variation of the Daytime Sextantids. The activity level has stayed flat in the past. The five years average shows a bigger change than the ten years and past average.

4.13.3 Discussion

The Meteor Shower Workbook 2022 (Rendtel, 2022) puts the peak at $\lambda_\odot = 184.°3$. The present study es-

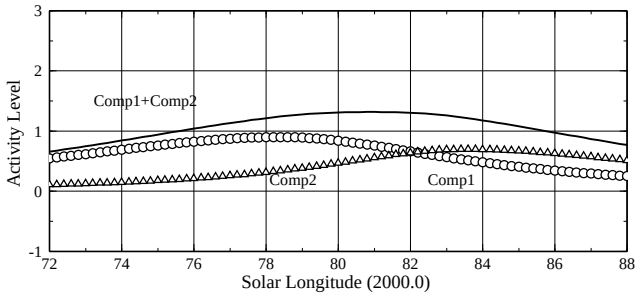

Figure 24 – Estimated components (circles refer to Comp1, triangles to Comp2 and the solid line to their sum.

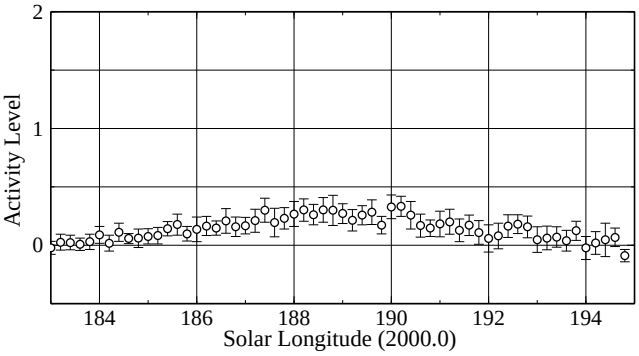

Figure 25 – The activity profile of the Daytime Sextantids in steps of 0.°2 in solar longitude, calculated using the Activity Level Index, and covering the period 2005–2022.

timates that the peak time was $\lambda_\odot = 188.°8$, which is much later. However, Ohtsuka et al. (1997) observed a peak at $\lambda_\odot = 188.°35$. CMOR radar data confirmed a peak time of around $\lambda_\odot = 187.°5$. SonotaCo Net video observations recorded the peak at $\lambda_\odot = 189.°2$ (Koseki, 2021).

5 Conclusion and Future work

The IPRMO succeeded to analyze the structure of meteor activity and annual variation by using worldwide radio meteor observations. By continuing to observe and analyze in the future, this has a potential for more long-term studies.

Nevertheless, some issues need to be resolved in the future.

First, changes in the annual variation of sporadic meteors must be studied. This is because the formula of the Activity Level Index considers the number of sporadic meteors ($H_{\mathrm{spo},i}$, $D_{\mathrm{spo},i}$). It therefore has to consider whether an increase of meteor echoes ($H_{\mathrm{obs},i} - H_{\mathrm{spo},i}$) means an increase of meteor shower activity or decrease of sporadic meteors when analyzing annual variation.

Second, most of the observing stations are located in the northern hemisphere. In this way, we may miss meteor shower activity in the southern hemisphere. Although it is very difficult to increase the number of observing stations in the world, the IPRMO will try to share knowledge and help beginners to start radio meteor observations.

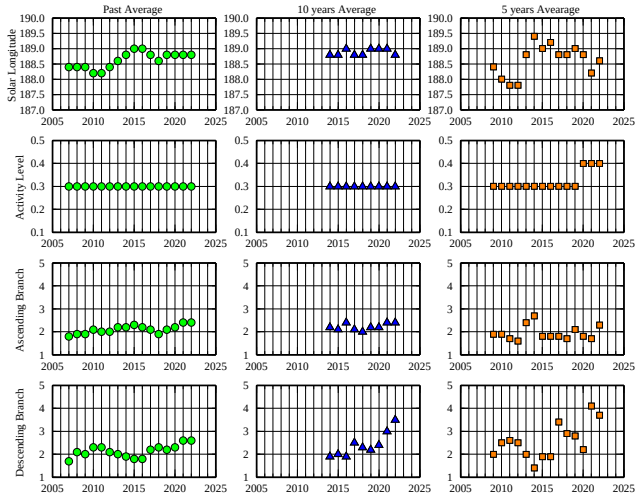

Figure 26 – The annual variation of the Daytime Sextantids (Top row: peak solar longitude, 2nd row: maximum Activity Level, 3rd row: duration of ascending branch, and bottom row: duration of descending branch. Left column: past average, middle column: 10 years average and right column: 5 years average.).

Acknowledgement

We wish to thank all radio meteor observers and Chris Steyaert and Pierre Terrier for providing and hosting the Radio Meteor Observation Bulletin. A very special thank you to Cis Verbeeck for his continuous support.

References

Arlt R., Rendtel J., and Bader P. (2008). "The 2007 Orionids from visual observations". *WGN, Journal of the IMO*, **36**, 55–60.

Brown P., Vaubaillon J., Jenniskens P., and Yrjola I. (2015). "Ursid meteors 2014". *Central Bureau Electronic Telegrams*, **4041**.

Dubietis A. and Arlt R. (2001). "Thirteen years of Lyrids from 1988 to 2000". *WGN, Journal of the IMO*, **29**, 119–133.

Jenniskens P., Crawford C., Butow S. J., Nugent D., Koop M., Holman D., Houston J., Jobse K., Kronk G., and Beatty K. (2000). "Lorentz shaped comet dust trail cross section from new hybrid visual and video meteor counting technique imprications for future Leonid storm encounters". *Earth, Moon and Planets*, **82-83**, 191–208.

Jenniskens P., Webb C. I., Kitting C., Peterson C. L., Miskotte K., and Vaubaillon J. (2008). "Perseid meteors 2008". *Central Bureau Electronic Telegrams*, **1480**.

Johannink C. (2013). "η Aquariids outburst 2013 observed by CAMS". *WGN, Journal of the IMO*, **41**, 199–200.

Koseki M. (2021). "The activity of meteor showers recorded by SonotaCo Net video observations 2007–2018". *eMetN*, **6**, 91–246.

McKinley D. W. R. (1961). *Meteor Science and Engineering*. McGraw-Hill Book Company, Inc.

Miskotte K., Sugimoto H., and Martin P. (2021). "The big surprise: a late Perseid outburst on August 14, 2021!". *eMetN*, **6**, 517–525.

Miyao K. and Ogawa H. (2004). "Research into the characteristics of meteor showers from multi-frequency radio observations". In *Proceedings of the International Meteor Conference, Bollmannsruh, Germany, September 19-21, 2003*. International Meteor Organization, pages 81–89.

Ogawa H. and Steyaert C. (2017). "Major and daytime meteor showers using global radio meteor observations covering the period of 2001-2016". *WGN, Journal of the IMO*, **45**, 98–106.

Ogawa H., Toyomasu S., Ohnishi K., Amikura S., Maegawa K., and Jenniskens P. (2002). "The 2002 Leonids as monitored by the International Project for Radio meteor Observations". *WGN, Journal of the IMO*, **30**, 225–231.

Ogawa H., Toyomasu S., Ohnishi K., and K. M. (2001). "The global monitor of meteor streams by radio meteor observation all over the world". In Warmbein B., editor, *Proceeding of the Meteoroids 2001 Conference, 6-10 August 2001*. Swedish Institute of Space Physics, Kiruna, Sweden. ESA Publications Division, European Space Agency, Noordwijk, The Netherlands, pages 189–191.

Ohtsuka K., Shimoda C., Yoshikawa M., and J. W. (1997). "Activity profile of the Sextantid meteor shower". *Earth, Moon, and Planets*, **77**, 83–91.

Rendtel J., editor (2014). *Meteor Shower Workbook 2014*. IMO.

Rendtel J., editor (2021). *2022 Meteor Shower Calendar*. International Meteor Organization. IMO_INFO 3-21.

Rendtel J., editor (2022). *Handbook for Meteor Observers*. IMO.

Rendtel J., Ogawa H., and Sugimoto H. (2017). "Meteor showers 2016: review of predictions and observations". *WGN, Journal of the IMO*, **45**, 49–55.

Steyaert C. (2014). "The global radio Eta-Aquariids 2013". In *Proceedings of the International Meteor Conference, Poznan, Poland, 22-25 August 2013*. International Meteor Organization, pages 73–77.

Uchiyama S. (2010). "Geminids ZHR activity profiles as a function of magnitude". *WGN, Journal of the IMO*, **38**, 31–35.

Guest Handling Editor: Cis Verbeeck
This paper has been typeset from a LaTeX file prepared by the author.

Ongoing meteor work

High inclination meteor showers in December and January

Jürgen Rendtel[1], *Sirko Molau*[2]

High inclination meteor showers produce annually well observable activity from early December to end January from the region Coma Berenices to Leo Minor. The observed parameters suggest that some of the streams listed in the IAU MDC data base are part of a complex stream, with some activity from other sources superposed. We find that the #0020 COM (Comae Berenicids) is the dominating source and thus also as the proper designation of the shower (complex). The activity is well detectable between December 4 ($\lambda_\odot = 251°$) and January 31 ($\lambda_\odot = 311°$). The shower is the strongest source in the northern sky from December 17 until end January except the Ursid and Quadrantid peak periods. The radiant at the reference position ($\lambda_\odot = 271°$) is $\alpha = 164°$, $\delta = +29°$, the atmospheric entry velocity is $V_\infty = 63\,\mathrm{km/s}$.

Received 2022 November 22

1 Introduction

Observers know that there are meteors radiating from northern positions in or near Coma Berenices primarily in December and well into January. Meteor shower lists include the Comae Berenicids with slightly enhanced activity usually around mid-December.

For many years, we listed two meteor showers in the IMO working list of meteor showers and therefore also in the annual IMO Meteor Shower Calendar. The data provided in the IMO publications were updated in 2010 and are based on an analysis of video meteor data (Molau & Rendtel, 2009). These seemed to confirm that the Comae Berenicids (#0020 COM) are active for a shorter period while the December Leonis Minorids (#0032 DLM) from a slightly further northern radiant can be traced from early December to early February. Both showers were also listed in the IAU MDC data base.

However, the #0032 DLM entry was deleted from the IAU MDC data base for some time, although meteor activity was reported by video and visual observations. A detailed analysis of meteor activity from the region was published by (Koseki, 2011), which he described as "Comae Berenicids and related activities". The data suggest that there is a complex of meteoroids on high inclination orbits which can be traced for a large fraction of the year.

The issue was raised again in a discussion by Peter Jenniskens proposing a new designation which describes the activity from the Coma Berenices – Leo Minor region in the sky. Since there are new rules about the designation of new showers (Rudawska et al., 2022), the suggested #1109 is not in the IAUMDC data base. The issue of the Coma Berenices showers was also discussed by (Koseki, 2009) in connection with old shower records.

In order to avoid confusion of the (visual) observers, the 2023 Meteor Shower Calendar describes the meteor activity as a complex with the (tentative) designation #0020 COM. Next, we try to sort the available data.

2 Radiants in the Coma Berenices – Leo Minor region in December to January

First, we check the entries of showers with radiants in the region Leo Minor to Coma Berenices listed in the IAU MDC data base for the period from mid-December to end-January (version accessed 2022 October 14).

In Table 1 (top part) we list all radiants found in the IAU MDC data base which are close to the region under discussion and with a geocentric velocity of at least 50 km/s, although in a strict sense we may restrict our search and attempt to group showers to showers with geocentric velocities of at least 60 km/s. (There are a few further entries but with significantly lower velocities and thus of different type, like the #0406 FCB February Comae Berenicids.) The second (lower) part of the Table 1 gives the three radiants quoted in (Koseki, 2011).

Data of the IMO Video Meteor Network (Molau & Rendtel, 2009) find the #0020COM and #0032DLM as published in the IMO Shower Calendar over the past years. However, this is not surprising if we look at the showers listed in Table 1 and radiants plotted in Figure 1. Further, there is no defined border or limit of a meteoroid stream and criteria for a suggested association can be defined and interpreted with some flexibility, depending on the available data or the intention of a search. The current IAUMDC data base adds two comments. In entry #0020COM: "Previously named December Leonis Minords", and in entry #0090JCO: "Duplicate name for shower 20, COM, between solar longitude 280 and 300".

The activity from the DLM/COM radiants is one of the longest meteor showers in our list. A recent analysis of single station video meteor data collected over 20 years aimed primarily at short duration meteor activity (presented by Sirko Molau at the on-line IMC 2021). The total sample for this shower search com-

[1]International Meteor Organization, Eschenweg 16, 14476 Potsdam, Germany. Email: jrendtel@web.de

[2]Abenstalstr. 13b, 84072 Seysdorf, Germany. Email: sirko@molau.de

IMO bibcode WGN-506-rendtel-com
NASA-ADS bibcode 2022JIMO...50..158R

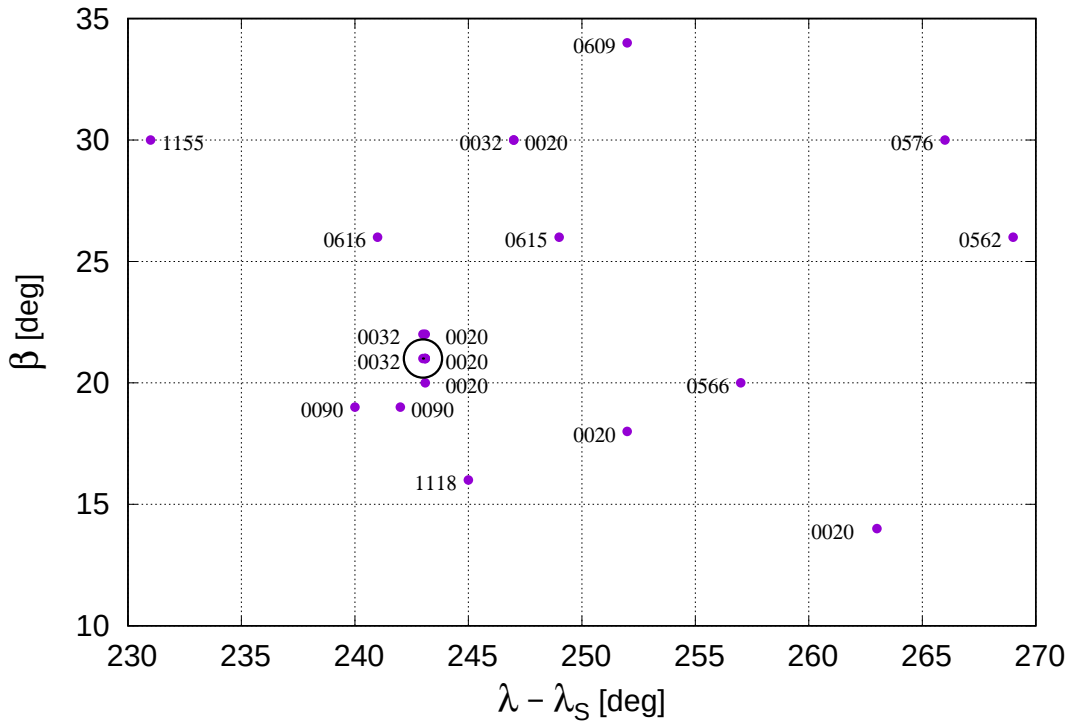

Figure 1 – Radiants in the region Coma Berenices to Leo Minor between early December and early February included in the IAU MDC data base (2022 October 14) in ecliptical coordinates (see Table 1). The circle at the 0032/0020 position in the centre marks the position we find from our radiant search procedure. It perfectly fits with the #0032DLM and #0020COM positions given in Table 1. The showers #0562, #0576, #0566, and #1155 are assumed to be not part of the suggested complex as their positions are quite far away from the other radiants.

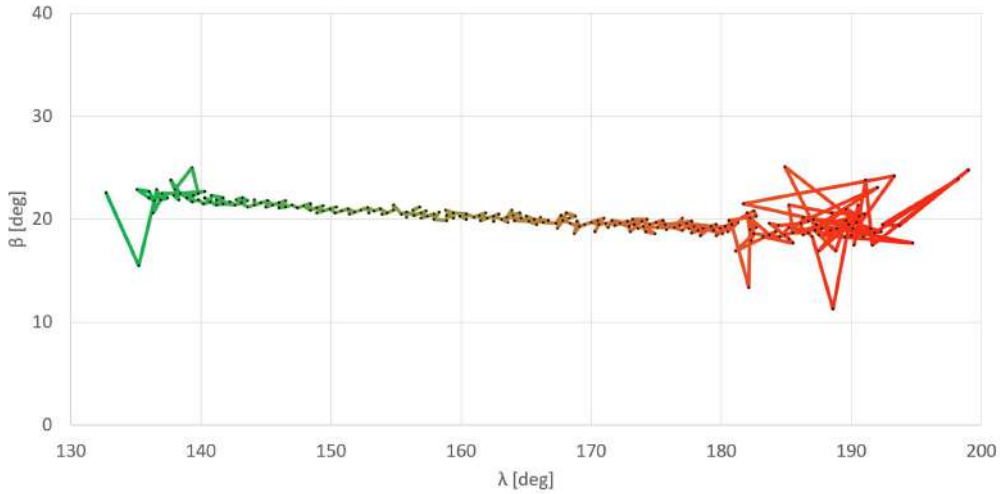

Figure 2 – Radiant of the Comae Berenicids as detected from the video meteor observations during the entire activity period. The solar longitude is colour coded; the motion is from left (green) to right (red). The increasing scatter at the start and particularly towards the end of the activity period is a result of the smaller number of meteors associated with the radiant under study and an indication that the activity period indeed starts and ends close to the dates given in Table 1 bottom line.

prised 4 051 360 meteors recorded between January 1993 and March 2019. For the search a bin size of 0.°2 in solar longitude and a shift of 0.°1 were used. Each solar longitude bin contains between 433 and 20 951 meteors. The radiant parameter space (α, δ, V_g) was sampled with 0.°5 resolution in position and 0.5 km/s in velocity. This search yielded 368 sources throughout the year. The result of the analysis of video data in the period we study here can be found at `https://www.imonet.org/showers/shw365.html`. It shows that the DLM/COM activity is emerging as early as December 4 ($\lambda_\odot = 251°$) from the background, and disappears only on January 31 ($\lambda_\odot = 311°$). Between December 17 and end of January it is the strongest source in the sky, only briefly interrupted by the Ursids and Quadrantids. Over 30 000 meteors from our database were assigned to the long-duration shower. The radiant coincides perfectly with the centre of the #0032DLM and #0020COM positions

Table 1 – Showers listed in the IAU MDC database (2022 October 14), sorted to the reference solar longitude. Please note that the data of (Koseki, 2011) (Table 4) refer to photographic work and to B1950.0 while the others refer to J2000.

#	Code	Name	$\lambda_\odot$ [°]	α [°]	δ [°]	λ [°]	β [°]	$\lambda-\lambda_\odot$ [°]	V_g [km/s]	i [°]	Reference
Entries in the IAU MDC data base (2022 Oct 14)											
1118	MLT	24 Leonis Minorids	259	152	29	144	16	245	65	146	SonotaCo et al., 2021
0619	SLM	7 Leonis Minorids	260	144	34	135	19	235	60	132	Šegon et al., 2014
0443	DCL	December Leonids	262	155	21	149	10	247	65	159	Shigeno & Yamamoto, 2012
0032	DLM	Dec. Leonis Minorids	262	156	33	145	21	243	62	134	Jenniskens, 2006
			262	164	40	149	30	247	64	138	Kashcheyev & Lebedinets, 1967
			268	162	31	151	22	243	64		Molau & Rendtel, 2009
0562	BCT	13 Comae Ber.	265	186	26	174	26	269	66	135	Andreić et al., 2014
0020	COM	Comae Berenicids	274	175	22	166	18	252	64	139	Jenniskens, 2006
			266	160	32	149	22	243	63	139	SonotaCo, 2009
			264	174	18	167	14	263	68		Molau & Rendtel, 2009
			276	169	27	159	20	243	67	137	Rudawska & Jenniskens, 2014
			277	170	27	160	21	243	63	135	Kornoš et al., 2014
			262	164	40	149	30	247	64	138	Kashcheyev & Lebedinets, 1967
			274	167	28	157	21	243	63	135	Jenniskens et al., 2016
1170	LTM	10 Leonis Minorids	277	144	36	134	20	217	51	83	Jenniskens, 2023
0566	BCF	5 Comae Ber.	278	184	20	175	20	257	67	143	Andreić et al., 2014
0576	FOB	40 Comae Berenicids	282	200	24	188	30	266	65	189	Gural et al., 2014
0319	JLE	January Leonids	282	148	24	142	10	220	53	109	Brown et al., 2008
			281	147	24	141	10	220	59		Molau & Rendtel, 2009
			282	148	24	142	10	220	52	108	Brown et al., 2010
			281	147	24	141	10	220	60		Molau et al., 2013
			283	148	24	142	10	219	51	100	Jenniskens et al., 2016
0609	BOT	37 Comae Berenicids	290	197	30	182	34	252	61	117	Šegon et al., 2014
0615	TOR	35 Comae Ber.	292	192	23	181	26	249	64	130	Šegon et al., 2014
0616	TOB	26 Comae Berenicids	300	192	23	181	26	241	61	124	Šegon et al., 2014
0090	JCO	Jan. Comae Ber.	301	189	17	181	19	240	64	137	Jenniskens, 2006
			304	193	15	186	19	242	66		Molau et al., 2013
1155	FBC	Febr. Beta Comae B.	314	197	25	185	30	231	55	104	Jenniskens, 2023
Showers according to Koseki (2011)											
0032	DLM	Dec. Leonis Minorids	262	156	32	146	21	244	62		Koseki, 2011
0020	COM	Comae Berenicids	283	172	25	162	20	239	62		Koseki, 2011
0090	JCO	Jan. Comae Berenicids	296	188	19	179	20	242	63		Koseki, 2011
Shower detected in the video meteor data of the IMO VMN											
0020	COM	Comae Berenicids	265	159	32	148	21	243	63		this work

Table 2 – Attempt to describe the radiants found in the Coma Berenices – Leo Minor region between early December to end January as one continuous source

$\lambda_\odot$	α	δ	#IAU
260	152	+29	1118
262	160	+35	0032
270	178	+27	0562, 0020
278	184	+20	0566
282	200	+24	0576, 0020
290	197	+30	0609
296	192	+23	0615, 0616
302	190	+16	0090
314	197	+25	1155

shown by the circle in Figure 1. Further, we find a very consistent radiant motion of $+0.96°/°(\lambda_\odot)$ in ecliptical longitude and $-0.05°/°(\lambda_\odot)$ in latitude (Figure 2) over the entire activity period. This is also reflected by a well-defined activity profile (Figure 3) with a slightly steeper ascending branch than the descending branch.

Table 3 – Radiants in the vicinity of the Coma Berenices – Leo Minor region between early December to end January which do not fit a continuous motion of a possible single source. This especially holds for the #0319 January Leonids with their well separated radiant position.

$\lambda_\odot$	α	δ	#IAU and remark
260	144	+34	0619 (northern position)
262	155	+21	0443 (southern position)
277	144	+36	1170 (far west and north)
282	148	+24	0319 (far west)

There are two dips in the shower activity relative to the sporadic activity at the Geminid peak and the Quadrantid peak. During these periods we find an increased number of major shower meteors which are erroneously taken as sporadic (small errors, too short trails close to the radiant). Hence the normalised activity becomes significantly lower.

The major feature of the activity profile is a relatively broad maximum between $\lambda_\odot = 265°$ and 277°. Similar results, except a clear timing of the maximum

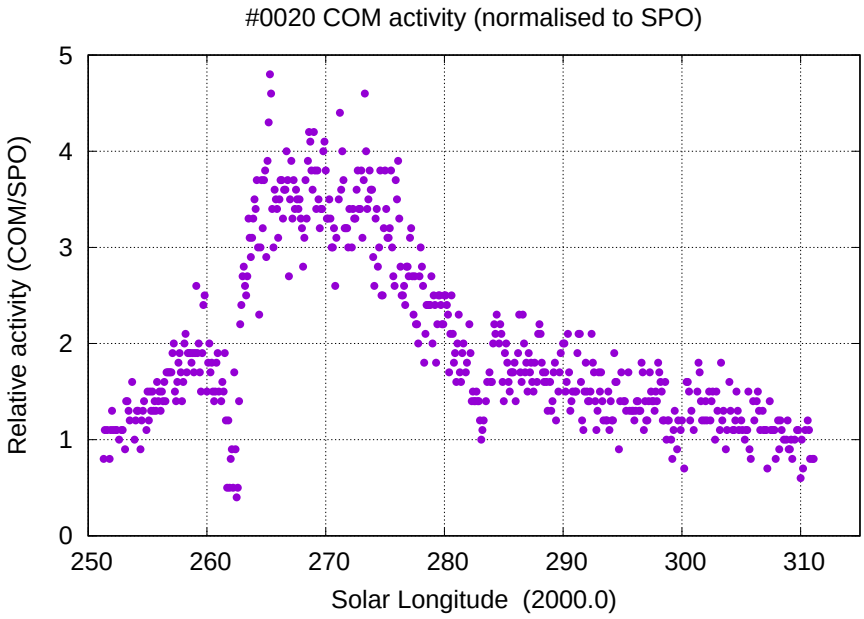

Figure 3 – Activity of the #0020 COM as given in Table 1, expressed as number of shower meteors relative to the number of sporadic meteors. The normalisation causes a decrease of the COM activity at the peaks of the two major showers, the Geminids and the Quadrantids. The reason is the large number of shower meteors, of which a fraction is erroneously is classified as sporadic. As a consequence, the ratio COM/SPO significantly decreases near 262° and 283° solar longitude.

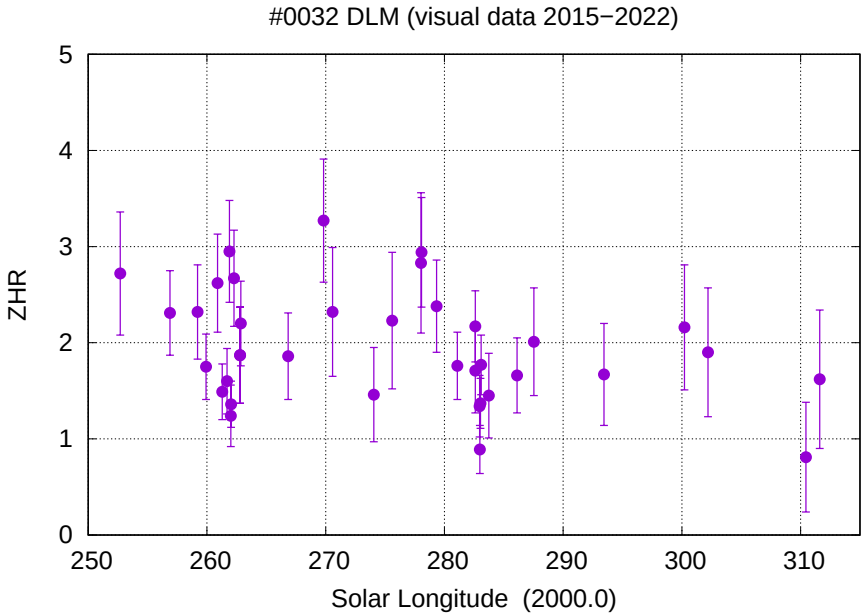

Figure 4 – ZHR of the long duration shower #0032 DLM (as assigned to the major activity in the IMO Meteor Shower Calendar over the period 2016–2022), assuming a constant $r = 3.0$. The graph shows all ZHR values obtained during the six returns. Values obtained close to the maximum times of the Geminids (262°) and the Quadrantids (283°) show significantly higher scatter likely caused by problems with the shower association during high activity.

activity, are found from visual data (Figure 4). Most likely, the higher rates remain unobserved visually due to the Christmas break in many regions. However, we also find effects of the major shower peaks on the ZHR values of the COM. The visual ZHR shows mainly a continuous activity which is slightly above the detection limit for visual observers.

The shower search procedure named the shower described above as #0032 DLM because that was the closest fitting radiant from the IAU MDC list, but this is arbitrary. If we assume $\lambda_\odot = 271°$ as the peak (reference) time, we find the radiant at $\alpha = 164°$, $\delta = +29°$ which is close to the border between Leo and Leo Minor, and less than 3° south of the star ξ UMa.

We compared the recent results with the result we published in 2009 (Molau & Rendtel, 2009). This earlier analysis yielded a similar activity interval ($\lambda_\odot = 253°$ to 315° with a peak at $\lambda_\odot = 268°$).

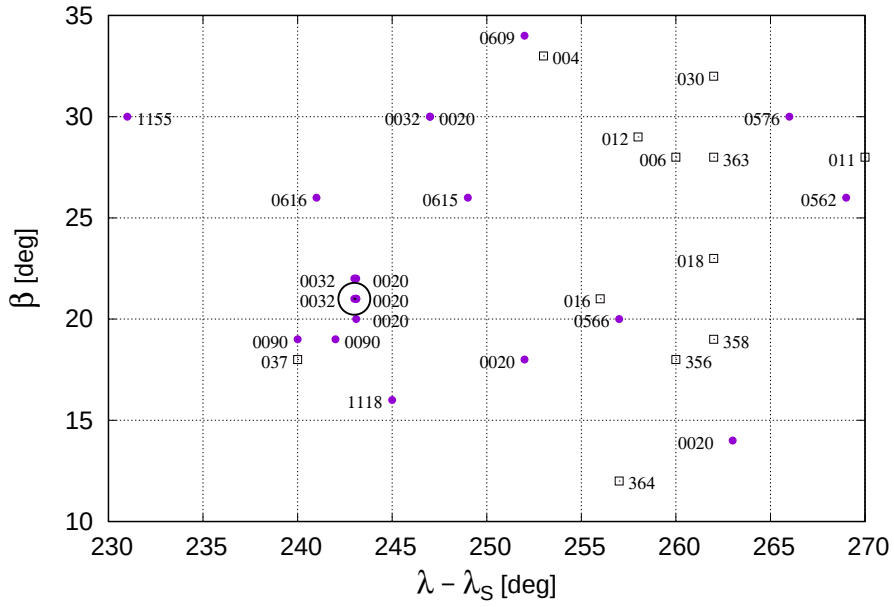

Figure 5 – The same region as shown in Figure 1 including the radiants discussed before (as dots with the 4-digit-IAU-numbers) as well as the radiants found in the stream search (given in Table 4, shown here as small squares with the 3-digit-numbers from the search procedure). Several sources occur at $\lambda - \lambda_\odot > 250°$, i.e. closer to the Earth's apex and a few are outside the plot. Perhaps only the 037 = #0506 FEV (February epsilon Virginids; established shower) may be associated with the #0020 COM discussed here. According to (Koseki, 2021) (especially pages 218–220) we may consider DLM, COM, JCO (and perhaps FEV) as a series of continuous meteor activity.

Table 4 – Radiants in the Coma Berenices – Leo Minor region between early December to end January found in the search for short-duration meteor activity presented at the IMC 2021 as explained in the text. Most of the radiants occur at $\lambda - \lambda_\odot > 250°$ (see also Figure 5). The number in the first column refers to the search and details may be accessed at `https://www.imonet.org/showers/shwxxx` with xxx the number given in the first column. The positions refer to the maximum of the detected activity. North/south describe the offset to the assumed "mean" radiant area.

Number in search	IAU MDC	$\lambda_\odot$ (Max.)	α [°]	δ [°]	λ [°]	β [°]	$\lambda - \lambda_\odot$ [°]	V_∞ [km/s]	Remarks
352	0339 PSU	252	168	44	149	36	258	60	north
356	0562 BCT	265	178	27	166	18	260	69	south
358	0562 BCT	268	180	22	170	19	262	69	south
363	0566 BCF	275	189	23	177	28	262	67	
364	0566 BCF	276	181	12	172	12	257	69	south
001	0319 JLE	282	148	24	142	10	220	58	slow
004	0576 FOB	285	192	30	178	33	253	63	
006	0576 FOB	286	197	23	186	28	260	66	
010	0609 BOT	289	212	31	196	40	267	65	north
011	0609 BOT	291	210	18	201	28	270	66	
012	0609 BOT	294	202	22	191	29	258	65	
016	0615 TOR	296	199	15	192	21	256	67	
018	0432 NBO	298	207	14	199	23	262	69	
019	0607 TBO	297	218	18	209	31	272	64	north
022	1103 FBI	299	217	5	213	18	274	69	south
025	0607 TBO	302	215	5	211	18	269	67	south
030	0620 SBO	306	218	19	208	32	262	64	
036	0620 SBO	312	223	22	213	36	262	63	
037	0506 FEV	312	198	12	192	18	240	65	

An attempt to describe the listed radiants as a consecutive sequence of one moving radiant cannot include all entries from Table 1. We may describe the activities in two different "groups" (Table 2). A continuously moving radiant which starts at $\lambda_\odot = 262°$ corresponds with the #0032 position as given by (Koseki, 2011), fits the #0020 position at $\lambda_\odot = 274°$ as well as the #0020 position (Koseki, 2011) and is finally at $\lambda_\odot = 300°$ close to the position of the radiants listed as #0090, #0615 and #0616. The average shift in degrees per 1° in solar longitude is $\Delta\alpha = 0.92$, $\Delta\delta = -0.24$ (or, if we restrict to the best defined period between $\lambda_\odot = 256°$ und 298°,

$\Delta\alpha = 0.88$, $\Delta\delta = -0.41$). The overall activity period covered by these radiant positions starts on December 4 and ends at January 31.

The shower search described above yielded 368 radiants during the entire year. Among these, we find the main source described here as well as a number of further activity sources listed in Table 4 – also shown in Figure 5 – which are relatively close to the #0020 COM. A few may be associated with the radiants listed in the previous tables but most of them are further east and probabbly do not belong to the complex discussed here.

3 Conclusions

If we indeed consider a solar longitude of $\lambda_\odot = 271°$ as a reference value, the corresponding radiant position is $\alpha = 164°$, $\delta = +29°$. This is closest to the #0020 COM entry given in Table 1. It is less than 3° south of the star ξ Ursa Major, north of the constellation Leo and east of Leo Minor. Again, if we take the date and position given above, the shower should be called ξ Ursae Majorids. But like in the case of the Quadrantids, we may keep the known disgnation and avoid further confusion.

Our normalised video meteor activity and ZHR (visual) data suggest that the COM activity is most obvious between December 17 and 29 ($\lambda_\odot = 265° - 277°$). The middle of this interval may be considered as reference date and is at December 23 ($\lambda_\odot = 271°$). Overall, the shower is detectable from December 4 ($\lambda_\odot = 251°$) until January 31 ($\lambda_\odot = 311°$).

The visual data of December 2019, 2020 and 2021 show no significant rate variation, but a trend to slightly higher ZHRs around December 20–23 similar to the video data.

Visual observations are not suited to distinguish between the individual radiants reported from different techniques, mostly video and thus with the possibility to separate the streams by orbital parameters. The conclusion for our own working list is that there is a long-lasting meteor activity from high-inclination showers. These can be grouped so that observers can provide shower magnitude data and rate informetion to derive ZHR and subsequently number densities or flux densities. in this respect it is helpful that the shower radiants are well separated from other active sources over the entire period and the high geocentric velocity is a unique characteristics.

Acknowledgement

We are grateful to Masahiro Koseki for his valuable additional information and fruitful discussions.

References

Andreić Ž., Gural P., Šegon D., Skokić I., Korlević K., Vida D., Novoselnik F., and Gostinski D. (2014). "Results of CMN 2013 search for new showers across CMN and SonotaCo databases I". *WGN, Journal of the IMO*, **42:3**, 90–97.

Brown P., Weryk R. J., Wong D. K., and Jones J. (2008). "A meteoroid stream survey using the Canadian Meteor Orbit Radar. I. Methodology and radiant catalogue". *Icarus*, **195:1**, 317–339.

Brown P., Wong D. K., Weryk R. J., and Wiegert P. (2010). "A meteoroid stream survey using the Canadian Meteor Orbit Radar. II: Identification of minor showers using a 3D wavelet transform". *Icarus*, **207:1**, 66–81.

Gural P., Šegon D., Andreić Ž., Skokić I., Korlević K., Vida D., Novoselnik F., and Gostinski D. (2014). "Results of CMN 2013 search for new showers across CMN and SonotaCo databases II". *WGN, Journal of the IMO*, **42:4**, 132–138.

Jenniskens P. (2006). *Meteor Showers and their Parent Comets*. Cambridge University Press.

Jenniskens P. (2023). *Atlas of Earth's Meteor Showers*. (in press).

Jenniskens P., Nénon Q., Albers J., Gural P. S., Haberman B., Holman D., Morales R., Grigsby B. J., Samuels D., and Johannink C. (2016). "The established meteor showers as observed by CAMS". *Icarus*, **266**, 331–354.

Kashcheyev B. L. and Lebedinets V. N. (1967). "Radar studies of meteors". *Smithsonian Contributions to Astrophysics*, **11**, 183.

Kornoš L., Matlovič P., Rudawska R., Tóth J., Hajduková, M. J., Koukal J., and Piffl R. (2014). "Confirmation and characterization of IAU temporary meteor showers in EDMOND database". In Jopek T. J., Rietmeijer F. J. M., Watanabe J., and Williams I. P., editors, *Meteoroids 2013*. pages 225–233.

Koseki M. (2009). "Meteor Shower Records: A Reference Table of Observations from Previous Centuries". *WGN, Journal of the IMO*, **37:5**, 139–160.

Koseki M. (2011). "Comae Berenicids and related activities". *WGN, Journal of the IMO*, **39:6**, 159–166.

Koseki M. (2021). "The activity of meteor showers recorded by SonotaCo Net video observations 2007–2018". *eMeteorNews*, **6:2**, 91–246.

Molau S., Kac J., Berko E., Crivello S., Stomeo E., Igaz A., Barentsen G., and Goncalves R. (2013). "Results of the IMO Video Meteor Network - January 2013". *WGN, Journal of the IMO*, **41:2**, 61–66.

Molau S. and Rendtel J. (2009). "A Comprehensive List of Meteor Showers Obtained from 10 Years of Observations with the IMO Video Meteor Network". *WGN, Journal of the IMO*, **37:4**, 98–121.

Rudawska R., Hajduková M., Jopek T., Neslušan L., Kokhirova G., and Koseki M. (2022). "The Two-Step Procedure for Naming Meteor Showers - New

Nomenclature Rules". In Pajer U., editor, *Proceedings IMC 2022, Poroszló, Hungary*. page submitted.

Rudawska R. and Jenniskens P. (2014). "New meteor showers identifed in the CAMS and SonotaCo meteoroid orbit surveys". In Jopek T. J., Rietmeijer F. J. M., Watanabe J., and Williams I. P., editors, *Meteoroids 2013*. pages 217–224.

Shigeno Y. and Yamamoto M.-y. (2012). "Meteor shower catalog based on 3770 triangulation analyses of double-station Image-Intensified video observations over Japan". *WGN, Journal of the IMO*, **40:1**, 24–35.

SonotaCo (2009). "A meteor shower catalog based on video observations in 2007–2008". *WGN, Journal of the IMO*, **37:2**, 55–62.

SonotaCo, Uehara S., Sekiguchi T., Fujiwara Y., Maeda K., and Ueda M. (2021). "J14: A Meteor Shower and Cluster Catalog". *WGN, Journal of the IMO*, **49:4**, 76–97.

Šegon D., Andreić Ž., Gural P., Skokić I., Korlević K., Vida D., Novoselnik F., and Gostinski D. (2014). "Results of CMN 2013 search for new showers across CMN and SonotaCo databases III". *WGN, Journal of the IMO*, **42:6**, 227–233.

Handling Editor: Javor Kac
This paper has been typeset from a LaTeX file prepared by the authors.

Meteor halo phenomena — attempt at a morphological classification

Peter C. Slansky[1]

Meteors can form very different types of halos around the meteor head. Since these halos are technically difficult to observe, there are only a few reports so far. In this article, seven observations of meteors showing different halo phenomena are presented. Two are from the author's own video recordings, five from recordings by others. These images are analysed and interpreted based on four basic facts about meteor halos. First, meteor halos are no hard bodies with sharp contours, their boundaries and transitions are fluid. Second, they are three-dimensional, transparent bodies, mostly with a rotational geometry. We look at them – and through them – from a certain observer's perspective from the outside. Third, meteor halos have an extremely high contrast that is not mastered by cameras. Image analysis must take into account overexposure artefacts. Forth, meteor halos are very short-termed. Using video technique, the effects of motion blur have to be taken into account. Using the images of the meteors with halos presented, the author develops a basic morphological model in three zones where four different types of meteor halos can occur. The inner zone A covers a volume with a radius of 1 to 100 m (in exceptions even more). The middle zone B has a radius of 1 to 10 km. Very bright flares and terminal flashes can occur here. The outer zone C goes up to a radius of 100 km and more around the meteoroid. Here, a widespread, faint, pale-blue afterglow can occur as a result of a terminal flash or flare. Without any doubt, all four halo phenomena considered in this system are causally interconnected.

Received 2022 October 27

1 Introduction

The knowledge about the morphology of meteors seems to be significantly concentrated on the longitudinal structures along the trajectory. "Meteor head", "wake", "green train", "persistent train" or "smoke train" are terms for such longitudinal components of meteors. The lateral components forming three-dimensional rotational bodies around the meteor head called "halos" have been reported and analyzed far less. Obviously, one reason is because they are so difficult to observe. Another reason is that they are so fluid: Halos do not show any hard border, just gradients. The phenomena of a "terminal flash" or of "flares" are connected with them. Moreover, halos have yet been observed only in fast meteors. The observation of meteor halo requires very high sensitive colour video cameras with, in some cases, high spatial and temporal resolution. But video meteor networks have long worked solely with black and white cameras with comparably low resolution. Also, there are some reports of visual sightings.[a]

The physical origin of meteor halos is still a subject of investigation and modelling (Vinković & Grisevich, 2020). Different scientific approaches for the explanation of meteors' light emissions have been made: electric charge and magnetic fields around the meteor head (Šiljić et al., 2018), UV-radiation (Jenniskens, 2004) or X-rays (Smirnov, 2015). Instead, there is not just one type of meteor halo, there are – at least – four types of meteor halos showing different colours, different dimensions and different temporal evolutions. Therefore, their respective luminous appearances could have different physical causes, which, however, are undoubtedly related to each other.

As an amateur meteor observer using colour video technology, I primarily take a morphological approach to the phenomenon of meteor halos. My main goal is to analyze the video images of individual examples of meteors showing significant halo formations as far as possible. To interpret these camera images correctly, we must remember four important things. First, meteor halos are no hard bodies with sharp contours. They are "luminous clouds" with more or less steep or flat brightness or colour gradients. So, their boundaries and transitions are fluid. It is not possible to measure the exact dimension of a halo, such as a precise radius. We can only determine approximate slopes. Second, they are three-dimensional, transparent bodies, mostly with a rotational geometry. We do not see a cross-section of them. We look at them – and through them – from a certain observer's perspective from the outside. Third, meteor halo phenomena go over an extremely high contrast range that is in its entirety not mastered by any existing camera. As a consequence, image analysis must take into account nonlinear overexposure artefacts. Forth, meteor halos are very short-term phenomena changing their shape, their brightness and their colour in very short time. Using video technique, we always have to consider the effects of motion blur due to the exposure time of a single frame. Taking these four facts into account, in this article I analyze some of my own video recordings of meteor halos as well as recordings by others. From this I derive a basic morphological classification of four types of meteor halos observed in three different geometric zones.

2 Observations of meteor halos

2.1 Own video observations

2.1.1 Perseid fireball 3414-2018

I observed Perseids 2018 from Geigersau, Bavaria, Germany, together with Bernd Gährken. On 2018 Au-

[1]IMO. Email: slansky@mnet-online.de

IMO bibcode WGN-506-slansky-halo
NASA-ADS bibcode 2022JIMO...50..165S

[a]Thomas Weiland, https://www.imo.net/members/imo_vmdb/view?session_id=77407

Figure 1 – Fireball 3414-2018 at its terminal flash. The bright star right of the centre of the image is Polaris, to the left of it the constellation UMi. The terminal flash produces strong overexposure of the image. But this does not mean that the large white area is to camera blooming alone: the terminal flash shows a spatial extension of up to 4 km radius. A strong green train can be seen and also the beginning of a green halo at the back of the terminal flash. Interestingly, the green train reaches into the bloomed area of the terminal flash. Because the green light of the green halo cannot "erase" white light of the terminal flash, there is the question if this indicates an axe-shaped inner halo. In addition to the median halos of the terminal flash with the green afterglow, all the sky background shows a pale blue outer halo. Please note that the right part of the image is from camera 1 with the terminal flash out of its field of view and the left part of the image is from camera 2 with the terminal flash in its field of view. So, the pale blue outer halo was detected by both cameras independently. Camera: Two Sony a7S at 25 fps and ISO 409.000, each with Canon FD 1.4/50 mm lens at $F = 1.4$.

Figure 2 – Fireball 3414-2018, one frame (= 0.04 s) after the terminal flash. The meteor head has proceeded a little bit further from the position of the terminal flash to the lower left. The strong green train can still be seen while the median halo now shows a strong green afterglow of the terminal flash. Still, all the sky background shows the pale blue afterglow. But its maximum brightness is not, as in the frame before, close to the meteor anymore but further outside.

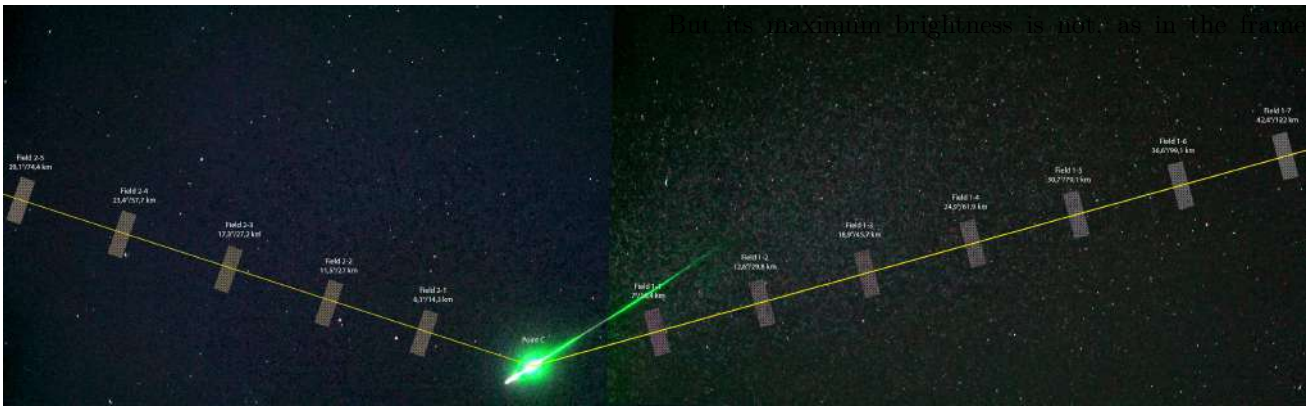

Figure 3 – Arrangement of the measurement fields for the blue afterglow in both camera fields. Measurement revealed that the pale blue afterglow lasted up to 12 frames (= 0.48 s) after the terminal flash. It appeared up to a lateral distance of more than 120 km from the center of the terminal flash, so it covered an air volume of more than 4.2 Mio. km^3 (Slansky & Gährken, 2019).

gust 13 at $01^h50^m58^s$ UT, two of my cameras – as well as two photo cameras of two other observers on another observation site – recorded a bright Perseid ending in a terminal flash.[b] It was assigned IMO fireball ID 3414-2018. The trajectory calculation by Jürgen Michelberger revealed an average geocentric speed of 60.6 km/s at a very steep entry angle. As a result, the meteoroid entered denser layers of the air rather swiftly. So, the terminal flash of 3414-2018 was very abrupt, showing a very sharp brightness peak.

Figure 1 shows 3414-2018 in the moment of the terminal flash: The peak brightness causes a certain blooming due to overexposure. But this does not mean that the large white area is to camera blooming alone.[c] The terminal flash shows a spatial extension of up to 4 km radius. A strong green train can be seen and also the beginning of a green halo at the back of the terminal flash. Interestingly, the green train reaches into the bloomed white area of the terminal flash. Because the green light of the green halo cannot "erase" white light of the terminal flash in the video image, there is the question if this indicates an axe-shaped inner halo. In addition to the median halos of the terminal flash with the green afterglow, all the sky background shows a pale blue outer halo. Please note that the right part of the image is from camera 1 with the terminal flash out of its field of view and the left part of the image is from camera 2 with the terminal flash in its field of view. So, the pale blue outer halo is detected by both cameras independently.

Figure 2 shows 3414-2018 one frame (= 0.04 s) after the terminal flash: The meteor head has proceeded a little bit further to the left from the position of the terminal flash. A strong green train can be seen. It is connected with a green halo around the position of the terminal flash. The rapid brightness decrease allows to see that the terminal flash is accompanied – respectively followed – by a widespread pale blue sky glow. Still, all the sky background shows the pale blue afterglow. before, close to the meteor anymore but further outside. All in all, the green afterglow had a duration of slightly more than one second. It lasts a little shorter than the green train, but it has exactly the same colour. The green afterglow has almost exactly the same dimensions as the terminal flash itself. Its centre is the point of the meteoroid at the moment of the terminal flash. Figures 1 and 2 show the interconnection between the green halo and the green train along the trajectory. The pale blue outer halo was measured up to a duration of 0.48 s (12 frames) after the terminal flash. It appeared up to a lateral distance of more than 120 km from the centre of the terminal flash and covered an air volume of more than 4.2 Mio. km^3 (Slansky & Gährken, 2019). Close inspection shows that the brightness of the pale blue afterglow slightly evolves from the centre to the periphery of the outer halo.

2.1.2 2014 Aurigid with terminal flash

On 2014 September 1 at $05^h44^m44^s$ UT, the author's camera recorded an Aurigid from La Palma ending in a terminal flash.[d] With an average speed of 66 km/s, the Aurigids are even faster than the Perseids. As there was no second observation of this meteor available its trajectory could not be calculated. Figure 4 shows just a sequence analysis: Just as with 3414-2018, the terminal flash of this Aurigid formed a short-lived white halo followed by a green afterglow halo of almost the same size. The green halo is connected directly to the green train, again. A widespread pale blue halo can only be seen very, very briefly. But it has to be taken into account that the camera had not been set to its maximum sensitivity and the iris of the lens was set to $F = 4.0$.

2.2 External observations in black-and-white

2.2.1 An early report

Andrei Ol'khovatov pointed me to a very interesting source. Ukrainian-Soviet Astronomer Igor Stanislavovich Astapovich (1908–1976) wrote in his standard

[b] Peter C. Slansky, `https://www.imo.net/members/imo_video/view?video_id=80`

[c] Empirical camera tests made by the author proved that these effects cannot be attributed to overexposure alone (Slansky & Gährken, 2018).

[d] Peter C. Slansky, `https://www.imo.net/members/imo_video/view?video_id=62`

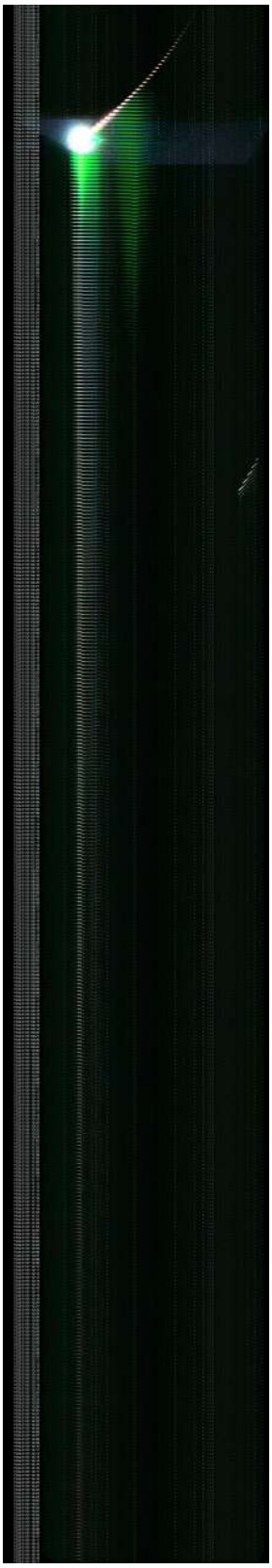

Figure 4 – Sequence analysis of an Aurigid on 2014 September 1 at $05^{h}44^{m}44^{s}$ UT from La Palma (Slansky & Gährken, 2019). The meteor flies from right to left. Each vertical step represents 1/25 s. Due to the exposure time of 1/25 s for each video frame there is significant motion blur. The terminal flash inside frame 6 is very abrupt. It is followed by a green halo with a duration of nearly one second. The green halo has direct connection with a faint green train. A widespread pale blue halo can be seen very briefly around the terminal flash. Camera: Sony a7S at 25 fps and ISO 204 000 with Zeiss ZE 2.8/35 mm lens at $F = 4.0$.

book "Meteor Phenomena in the Earth's Atmosphere" ((Astapovich, 1958); title translated[e]) on page 448:

> § 291. A 'violet halo' accompanies the flight of very bright meteors (see Figure 215). Its presence indicates a significant role of ultraviolet radiation, apparently causing the surrounding air within a radius of several kilometres to fluoresce (resonance excitation), as in some explosions.[f]

Figure 215 on page 441 shows a black and white photograph taken via a rotating shutter of a meteor with a dim halo. The original image subtitle reads: "Orionid 19th October 1952. The halo (fluorescent coloured) has a diameter of 3 km (AAL photo)."

It is important to keep in mind that the diameter measurement of a halo or of any other light effect in a photographic image is strongly dependant on the sensitivity of the photographic system. Unfortunately, Astapovich did not give any reference either to the technical background of his diameter measurement nor to the photographic technique used in this image. But on page 138 Astapovich states that the first colour photo of a meteor in the Soviet Union had been taken in 1955, three years after that 1952 Orionid. Hence, questions can be raised: how did he distinguish the "violet" or "fluorescent" colour of the halo? Certainly not from a black-and-white photo. A visual observation of this meteor is not reported. But even if there had been one: the human eye is very insensitive for dim and short time colour phenomena. Therefore, I assume Astapovich selected the designation "violet" and "fluorescent coloured" for the halo due to his assumption of ultraviolet radiation and fluorescence as the physical reasons. We might call this speculative. After all, this is the first source about a meteor halo I have found. As we will see later, this is most likely an example of a median meteor halo. The halo photographed is probably a green afterglow. Green being the complementary colour to violet makes for a nice punchline.

2.2.2 The 2001 "high-speed-Leonid"

The most prominent example of a meteor with a halo was a 2001 Leonid reported by Stenbaek-Nielsen and Jenniskens (Stenbaek-Nielsen & Jenniskens, 2003). The video recording had been made with a black-and-white image-intensified high speed camera at 1000 fps. Due to the short exposure time of only 1 ms there was no visible motion blur. The video frames show an "axe-shaped" or "bow-like" halo structure close to the meteor head with a radius of up to some 100 m. As the camera was equipped with a high speed lens of comparably long focal length its field of view was only $6.4° \times 6.4°$. These images induced a lot of articles to various meteor related topics and it inspired theory building of meteor halos

[e] Unfortunately, I am not able to read Astapovich's book in the original Cyrillic Russian. Therefore, I am highly grateful to Ms. Irina Boyarchuk, guest student from the Ukraine at my University, for her translation.

[f] Astapovich's original term "взрывах" might not only refer to "explosions" but also to terminal flashes and flares.

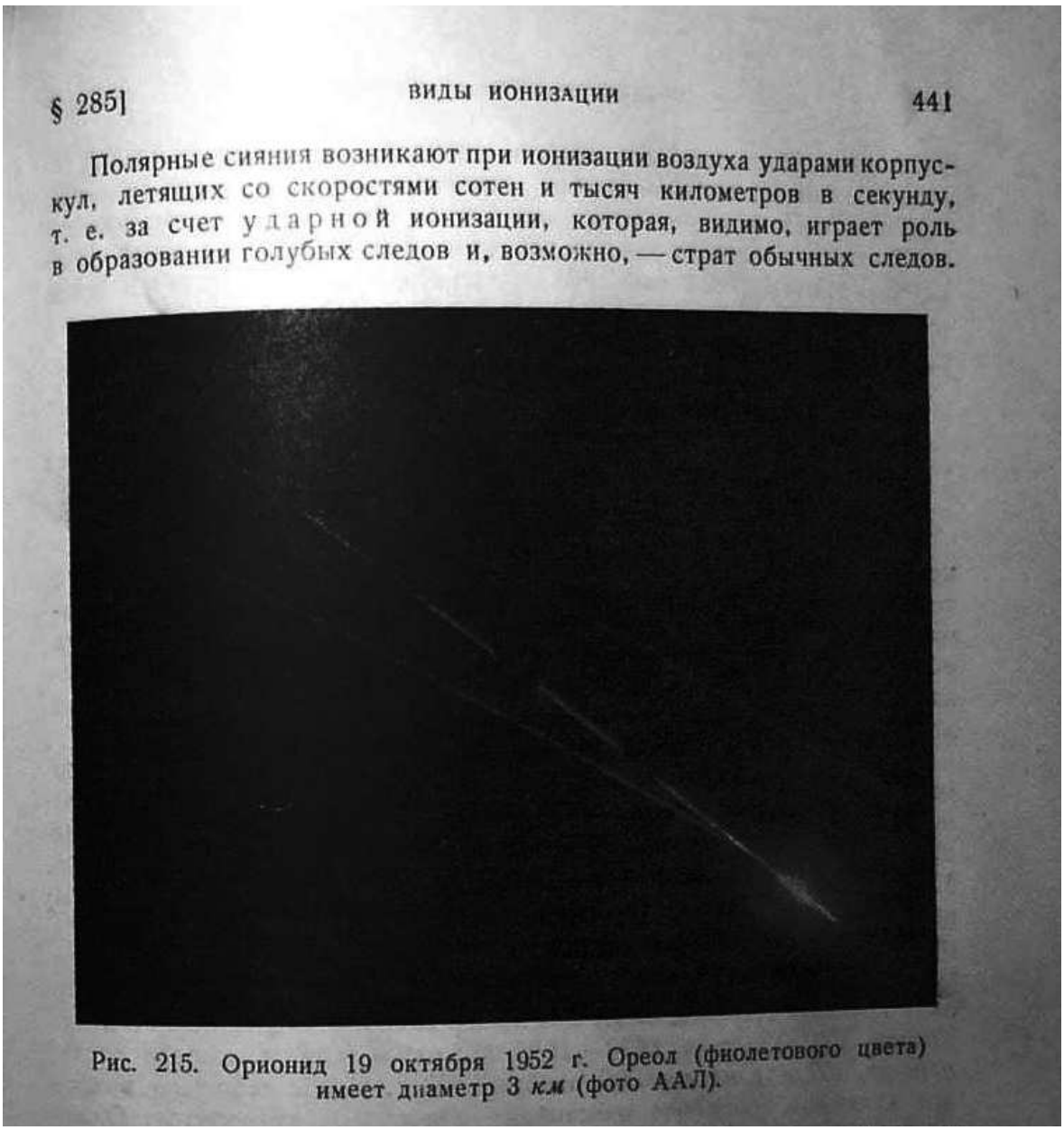

Figure 5 – "Figure 215" on page 441 of Astapovich's book (Astapovich, 1958); original subtitle: "Figure 215: Orionid 19th October 1952. The halo (fluorescent coloured) has a diameter of 3 km (AAL photo)." Earlier Astapovich states that the first colour meteor photo in the Soviet Union was taken only in 1955. So, this photo must have been taken on black and white film.

like hardly any other observation of a single meteor. So, we have to really call this high-speed Leonid video a lucky strike.

To my knowledge, this 2001 high-speed Leonid is the only photographically documented example of a narrow meteor halo. On the IMC 2018 I had a discussion with Peter Jenniskens about the question if 3414-2018 also shows signs of a similar narrow halo. However, we did not come to a definitive conclusion. In Figure 1, the beginnings of an "axe"-shaped halo can be seen, but only very vaguely.

Subsequently, I dedicated the observation of the 2019 Perseids, during which the full moon interfered strongly, to the hunt for narrow meteor halos with short exposure times. I used the "head hunter's quad" (not to be confused with "head hunter squad"): four Sony a7S cameras with 1.4/85 mm lenses.[g] All four cameras were operated at their maximum ISO value with an exposure time of 1/1000 s (= 1 ms). But this campaign was unsuccessful. Within 2:42 hours, the four cameras recorded 50 meteors altogether, including 44 Perseids, but there was no bright meteor with a visible halo among them.[h]

2.3 Video recordings of meteor halos by the AllSky7 network

Obviously, the blue afterglow can only be detected with very sensitive colour video cameras. In the meantime more colour video recordings of meteors' terminal

[g]Peter C. Slansky, https://www.imo.net/members/imo_photo/view?photo_id=1222

[h]Peter C. Slansky, https://www.imo.net/members/imo_photo/view?photo_id=1265

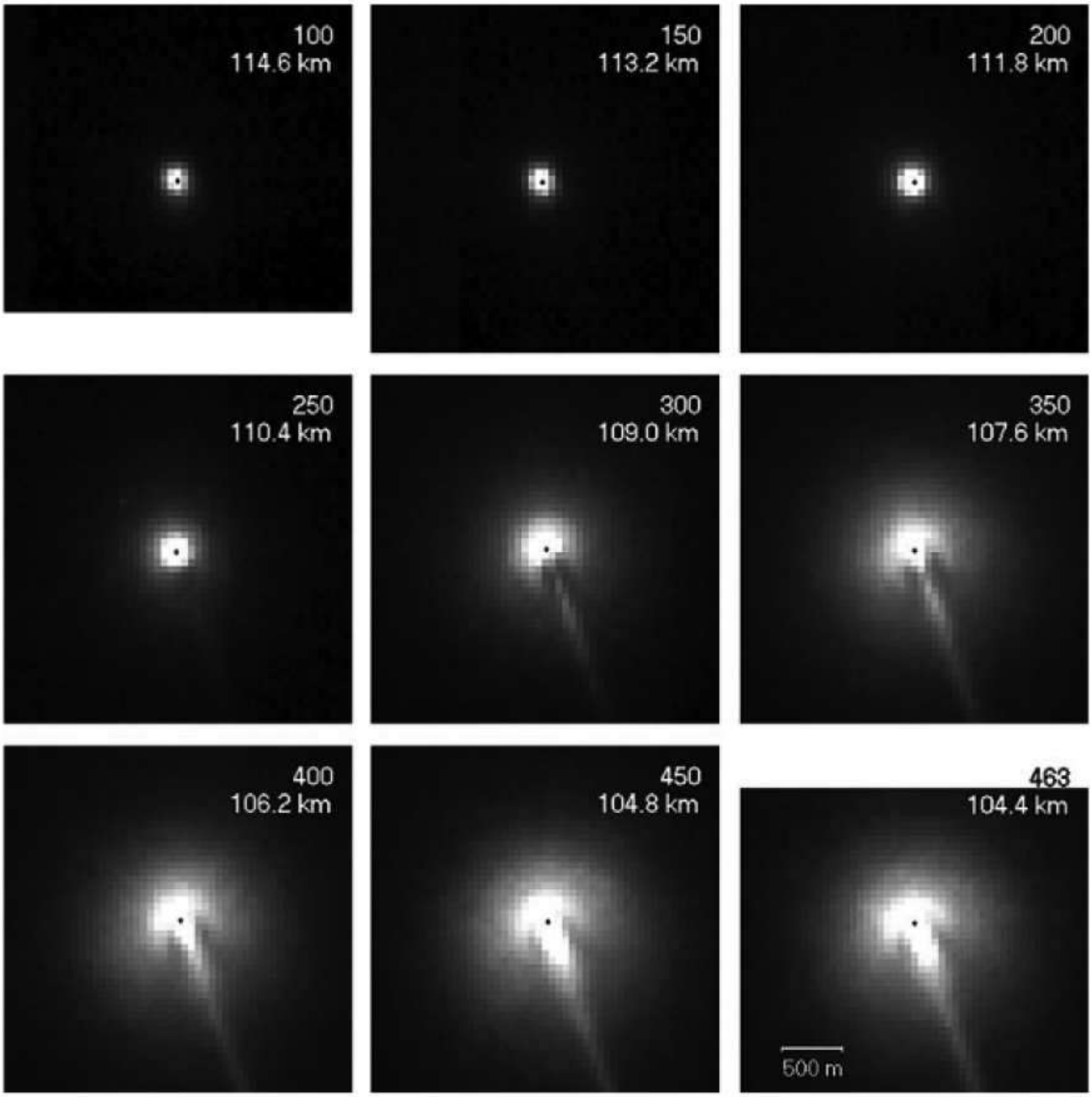

Figure 6 – 2001 Leonid; selected frames from a high-speed video sequence. Each image is a 1 ms exposure. The fitted meteor position is shown, the frame number and the altitude are indicated.

flashes with a blue afterglow have been made. With the AllSky7 network, colour video camera stations have been released in great number in the last four years. The brightest fireballs are available online via the AllSky7 Fireball Network Archive.[i] Each AllSky7 station contains seven cameras, each with a field of view of 45° × 80°. Figures 7 to 14 show the video frames of one of the seven cameras. The AllSky7 camera systems have a semi-automatic exposure control and an automatic white balance. For further research, the cameras' opto-electronical conversion function could be determined and a photometry and colourimetry of the videos could be made.

In the AllSky7 fireball network archive I found six fireballs that showed a terminal flash with a blue afterglow, all of them recorded by more than one camera. The three examples with the most significant outer halo showing a blue afterglow are fireball IMO ID 7242-2021, recorded by Jim Rowe in Eastbourne, UK,[j] fireball 3542-2022, recorded by Ranjit Biswas in Kolkata, India,[k] and, top of the list, fireball 2406-2021,[l] recorded by Sirko Molau in Conow, Germany.

[i] AllSky7 Fireball Network Archive, `https://allsky7.net/#archive`

[j] AllSky7 Fireball Network Archive: 2021-11-03, 21:34:39 UT, IMO Fireball ID: 2021/7242, `https://allsky7.net/archive.html?date=20211103&time=213439`

[k] IMO fireball archive: 2022-05-26, 19:21 UT, IMO Fireball ID: 3542-2022, `https://www.imo.net/members/imo_video/view?video_id=212`

[l] AllSky7 Fireball Network Archive: 2021-04-23, 01:30:35 UT, IMO Fireball ID: 2021/2406, `https://allsky7.net/archive.html?date=20210423&time=013035`

Date Time (UT)	AMS File Name IMO Fireball ID	Station	Main Observer	Significance	Reference
23.04.2021 01:30:35	AMS35_20210423_013035_7 2406-2021	Conow/DE	Sirko Molau	+++	[l]
03.11.2021 21:34:39	AMS117_20211103_213439_5 7242-2021	Eastbourne/UK	Jim Rowe	++	[j]
26.05.2022 19:21:33	AMS138_20220526_192133_7 3542-2022	Kolkata/IN	Ranjit Biswas	++	[k]
07.12.2021 17:29:00	AMS90_20211207_172900_1 —	Györ/HU	Zsolt Kereszty	+	[m]
20.10.2021 16:28:07	AMS71_20211020_162807_2 6766-2021	Becsehely/HU	Krisztián Sárneczky, Balázs Csák	+	[n]
05.02.2021 17:08:37	AMS54_20210205_170837_1 715-2021	Benediktbeuern/DE	Stephan Adler	+	[o]

2.3.1 Fireball 2406-2021

Recorded by AMS35/Sirko Molau on 2021 April 23, $01^h30^m35^s$ UT, in Conow/Germany.

Fireball 2021-2406 shows an exceptional peak brightness coming with a broad peak light curve. Although AllSky7 camera systems have a semi-automatic exposure control and an automatic white balance a brief colour measurement could be made. First signs of a pale blue outer halo begin in Figure 7, 12 frames (= 0.48 s) before peak brightness. The meteor head becomes so bright that the image begins to show blooming. The wake can be seen as well as the beginning of a faint green train. In Figure 8, 6 frames (= 0.24 s) before the terminal flash, the meteor head has become so bright that the image blooming gets stronger. It covers the wake and the green train. The sky background is brightened. As a consequence of a lens artefact, radial "rays" appear around the meteor head.

In Figure 9, 4 frames (= 0.16 s) before the terminal flash, the meteor head has become so bright that the image blooming now covers a large radius. The radial "rays" have become stronger. The sky background is brightened, but not only due to overexposure but also to the beginning of a pale blue outer halo. Figure 10 shows the terminal flash with peak brightness. The terminal flash is so bright that the image is completely overexposed. Dimensions of halo structures cannot be determined. The pale blue outer halo has become brighter. In Figure 11, 3 frames (= 0.12 s) after the terminal flash, the pale blue outer halo is very prominent. In Figure 12, 6 frames (= 0.24 s) after the terminal flash, the colour of the pale blue afterglow reaches its peak saturation but its brightness has fallen of a little bit. In Figure 13, 12 frames (= 0.48 s) after the terminal flash, the outer pale blue halo can still clearly be seen covering all the field of view of $45° \times 80°$. In this video it could be detected up to 19 frames (= 0.76 s) after the terminal flash, even longer than 3414-2018 with 0.48 s. In Figure 14, 32 frames (= 1.28 s) after the terminal flash, the outer pale blue halo has vanished. There is no green train anymore and no green afterglow. We still see a median white halo that transforms to a persistent train in the following. It must be noted, however, that 2406-2021 shows a very broad brightness peak, while 3414-2018 shows an abrupt one, so, the decay time of the pale blue afterglow might well be the same. Nevertheless, the light development of 2406-2021 is the most significant example for an outer halo with a pale blue afterglow I have seen yet.

2.3.2 Fireball 7242-2021

Recorded by AMS117/Jim Rowe on 2021 November 3, $21^h34^m39^s$ UT, in Eastbourne/UK.[j]

Despite some sky brightening, this fireball shows multiple flares with a green afterglow as a median halo and with a pale blue afterglow as an outer halo.

2.3.3 Fireball 3542-2022

Recorded by AMS138/Ranjit Biswas on 2022 May 26, $19^h21^m33^s$ UT, in Kolkata/India.[k]

This fireball shows a multiple flare which comes together with green afterglow as median halo, some of them showing a widespread pale blue-green afterglow as an outer halo. Its colour is shifted to green very strongly, obviously due to a shift of the camera's white balance.

2.4 Summary from the observations

As I had pointed out earlier, we often use terms like "meteor head", "wake" or "train" – even "halo" – as if a meteor consisted of several, sharply separated individual parts. But this is not the case. Only the meteoroid itself is a solid body with sharp defined form. But the meteoroid we cannot see. All visible light appearances of the meteor are gas or plasma phenomena with more or less significant brightness gradients, which, moreover, as a rule, overlap. Therefore, the sensitivity, dynamics and resolution of our imaging systems strongly determine the reproduction of the parts of the meteor in the image. For example, the track of a meteor will be longer in an image taken with a more sensitive camera than with a less sensitive one. The same applies to the "radius" of a halo around a meteor head: Since, as we have seen, the halo is not a sharply defined solid body, the term "radius" refers only to the visible radius in the image down to the sensitivity threshold of the imaging system. In reality, the halo is larger, but according to the brightness gradient, it can no longer be detected by

Figure 7 – Fireball 2406-2021, 12 frames (= 0.48 s) before the terminal flash. The meteor head becomes so bright that the image begins to show blooming. The wake can be seen as well a very faint green train.

Figure 8 – Fireball 2406-2021, 6 frames (= 0.24 s) before the terminal flash. The meteor head has become so bright that the image blooming gets stronger. It covers the wake and the green train. The sky background is brightened. As a consequence of a lens artefact, radial rays appear.

the camera system further away from the centre. When it comes to colour, it is even worse: with highly saturated, overexposed colours, cameras can produce very strange-looking artefacts.

Despite all the technical limitations of those days, the first photographic documents of meteor halos (see Astapovich) appeared as early as 70 years ago. But in the meantime only comparatively few have been added. With today's ultrahigh light-sensitive colour video cameras the temporal development, the colours and the structures of these halos can be investigated in detail. A few examples could also be recorded by the author. The formation of a halo around a meteor head has been studied by several authors, including Šilić et al., Jenniskens and Smirnov, but also Astapovich. Another very exciting discovery made by Obenberger et al. is

Figure 9 – Fireball 2406-2021, 4 frames (= 0.16 s) before the terminal flash. The meteor head has become so bright that the image blooming now covers a large radius. The radial rays have become stronger. The sky background is brightened, but not only due to overexposure but also to the beginning of a pale blue outer halo.

Figure 10 – Fireball 2406-2021, terminal flash/peak brightness. The terminal flash is so bright that the image is completely overexposed. Dimensions of median halos cannot be determined. The pale blue outer halo has become brighter.

that fireballs can also emit radio pulses with a duration of 10 s of seconds (Obenberger et al., 2014).

3 Morphological classification model of meteor halos

Based on the observations presented here, I propose to differentiate between three different zones where four different types of halos can occur. All four types of halos are interconnected causally.

Zone A marks a radius around the meteoroid of about 1 to 100 metres (in rare examples even more). Here an axe-shaped inner halo or "shock-front-halo" can occur. One example is the famous 2001 high-speed Leonid. In zone A, halo formation is presumably caused

Figure 11 – Fireball 2406-2021, 3 frames (= 0.12 s) after the terminal flash. The pale blue outer halo is very prominent.

Figure 12 – Fireball 2406-2021, 6 frames (= 0.24 s) after the terminal flash. The colour of the pale blue afterglow reaches its peak saturation but its brightness has fallen of a little.

mainly by aerodynamic processes resulting from ablation (Silber et al., 2018).

Zone B marks a radius of a few km around the meteoroid. Here, flares and terminal flashes may occur as median halos, possibly accompanied by a green afterglow of about the same dimensions. Some examples of these have been examined in this article. The main physical reasons for the halo formation in this zone are still unclear. It seems hard to believe that from the very small meteoroid a physical transport of material is possible to distances of some kilometres. Although a terminal flash looks similar to an explosion, it would then rather be a fast luminous wave front. There is also the question of whether, in the case of particularly large and fast meteoroids, the inner halo from zone A can extend so far that it reaches into zone B.

Zone C marks a volume outside of Zone B of up to more than 100 km radius around the meteoroid. Here

Figure 13 – Fireball 2406-2021, 12 frames (= 0.48 s) after the terminal flash. The outer pale blue halo can still clearly be seen covering all the field of view of $45^\circ \times 80^\circ$.

Figure 14 – Fireball 2406-2021, 32 frames (= 1.28 s) after the terminal flash. The outer pale blue halo has vanished. We see a median halo with a white afterglow that forms a persistent train. There is no green train anymore and no green afterglow.

the pale blue afterglow can occur as a result of a flare or terminal flash. After 3414-2018 there have now been more observations by cameras of the AllSky7 network. So, the phenomenon of the pale blue afterglow is proved to be real. The dimensions of these outer halos with more than 100 km radius and an atmospheric volume covered of several Mio. km^3 are really impressing. As the colour is a pale, desaturated blue, it cannot go back to emission at a single wavelength as with the green afterglow. Obviously, metastable states of the molecules and atoms in the atmosphere play a major role. But how are they induced, how is the energy transferred over hundreds of kilometres? Also, the geometry of the outer halo should be investigated further. We have to take into account that the earth's atmosphere has a vertical structure that changes significantly at an altitude

Figure 15 – 7242-2021, in the moment of peak brightness. Despite some sky brightening, a widespread pale blue outer halo can well be seen.

Figure 16 – 3542-2022, two frames after a flare. The outer halo is extremely wide showing a blue-green colour.

of 80 – 115 km. Therefore, the very simple model of a sphere with a radius of up to over 100 km and a certain decrease in brightness from the centre to the periphery can only be a first draft. There are more questions: What function does the decrease follow? What, if the observer is inside the halo? What role does the transparency of the Earth's atmosphere play? What temporal function does the decay of the afterglow follow?

I expect that the physical origins of all halo phenomena a meteor can show are directly related to each other. Today meteor halos appear to be a rare phenomenon. But it may well turn out that they are just a *rarely observed* phenomenon. It might even turn out that all meteors have some kind of halo that we just can't observe (yet).

4 Summary

More video observations are necessary to understand the morphology of meteor halos better. Unfortunately,

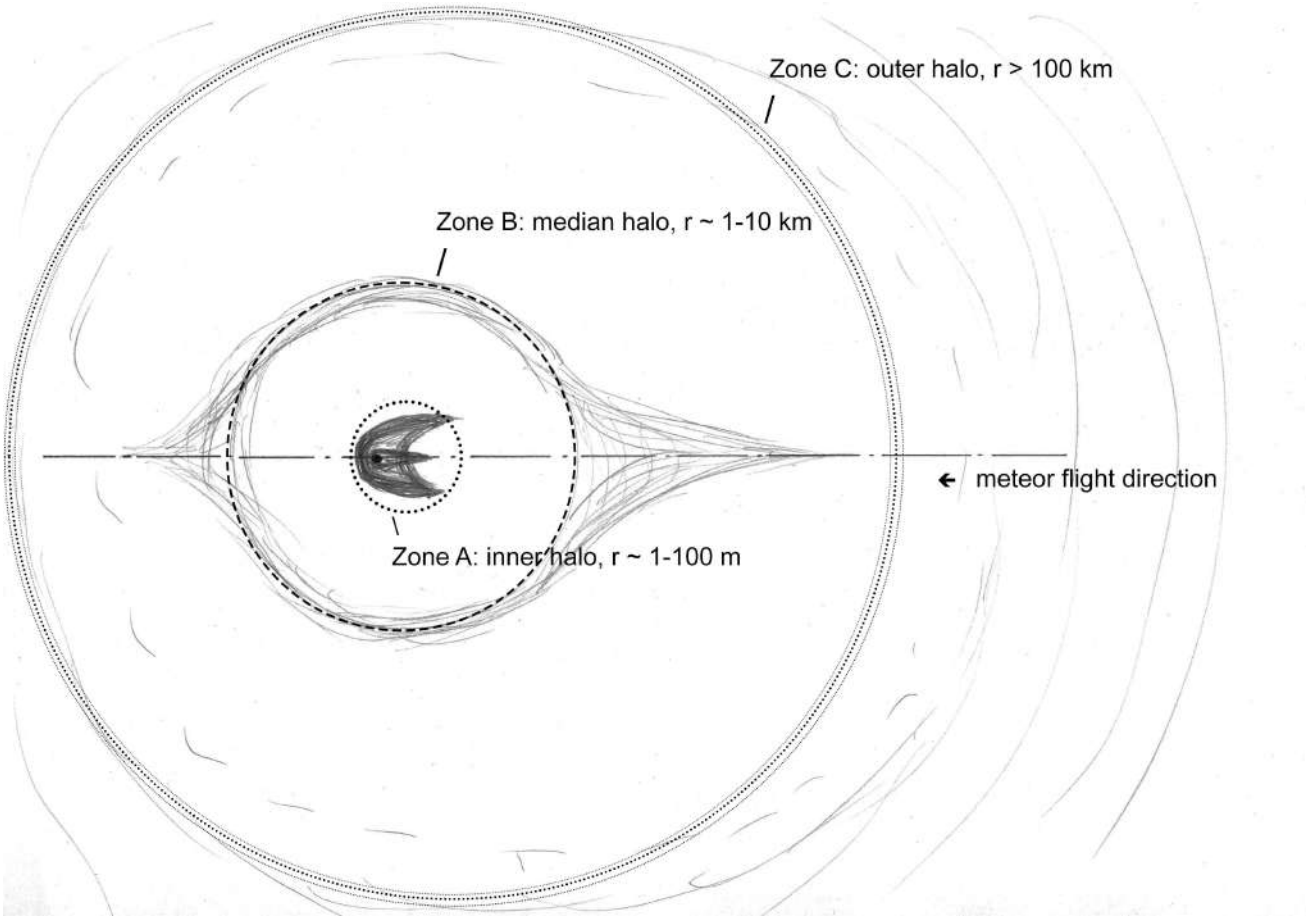

Figure 17 – Sketch of a morphological classification model of meteor halos in three zones (cross-section). Attention: The sketch is not to scale. Zone A marks an inner halo with a radius of approx. 1 up to 100 m. This may be for example a shock front in form of an axe or bow. Zone B marks a median halo. Here a terminal flash (white) may occur which sometimes may show a green afterglow. Due to the same colour the green afterglow is likely to have the same reason as the green train: the forbidden oxygen emission line at 557.7 nm. Zone C marks an outer halo with a radius up to 100 km and more. Here a pale blue afterglow of a terminal flash or flare can appear. Note that the radius factor between the inner and the median halo is about 10^2, as well as between the median and the outer halo.

the different types of halos require different observations techniques. For inner halos (zone A) a very short exposure time, a high spatial resolution and a high magnification are key. Colour is mandatory. Median halos (zone B) need a medium field of view and medium sensitivity but colour. For the green afterglow narrowband filters might be used. The outer halo (zone C) requires very high sensitivity and very wide field and colour, again. Spectroscopy seems impossible due to the low light level. For zones B and C multi station observations and trajectory calculations are highly valuable. In this case, small sensor cameras have an advantage over large sensor cameras (usually preferred by the author): they have lenses with shorter focal length and, as a consequence, faster F-stops available. From the perspective of photography a meteor halo is not a point shaped phenomenon but a planar one, so, the F-stops of the lens is key, not the entry pupil. Hence, lenses with fast F-Stop and wide field are favourable for observations of outer meteor halos.

Acknowledgements

I want to say thank you to Andrei Ol'khovatov, Russia, for pointing me to Astapovich's book, Irina Boyarchuk, Ukraine, for her translations, Bernd Gährken, Germany, for his support at the observation and the analysis of fireball 3414-2018, Peter Jenniskens, USA, for his feedback to my fireball videos, Thomas Weiland, Austria, for his descriptions of visual observations of meteor halos and Sirko Molau, Germany, for his technical information about the AllSky7 camera system.

References

Astapovich I. S. (1958). *Meteor Phenomena in the Earth's Atmosphere [translated].* State Publishers of Physical-Mathematical Literature, Moscow.

Jenniskens P. (2004). "Meteor storms as a window on the delivery of extraterrestrial organic matter to the early Earth". In Norris R. P. and Stoothman F. H., editors, *Bioastronomy 2002: Life among stars, IAU Symposium*, volume 213. IAU, pages 281–288.

Obenberger K. S., Taylor G. B., Hartman J. M., Dowell J., Ellingson S. W., Helmboldt J. F., Henning P. A., Kavic M., Schinzel F. K., Simonetti J. H., Stovall K., and Wilson T. L. (2014). "Detection of radio

emission from fireballs". *The Astrophysical Journal Letters*, **788:L26**, 6pp.

Silber E. A., Boslough M., Hocking W. K., Gritsevich M., and Whitaker R. W. (2018). "Physics of meteor generated shock waves in the earth's atmosphere – a review". *Advances in Space Research*, **62:3**, 489–532. (DOI: https://doi.org/10.1016/j.asr.2018.05.010).

Šiljić A., Lunić F., Teklić J., and Vinković D. (2018). "Proton-induced halo formation in charged meteors". *MNRAS*, **481**, 2858–2870.

Slansky P. C. and Gährken B. (2018). "Camera test of the Sony a7S with a Canon FD 1.4/50 mm lens about blooming of overexposed highlights in regard of the video observation of fireball 3414-2018". http://slansky.userweb.mwn.de/bereiche/astronomie/aufnahmetechniken/bilder/camera-test_sony-a7s_3414_2018.pdf .

Slansky P. C. and Gährken B. (2019). "3414-2018: A perseid fireball showing exceptional light effects, observed by video, photo and radio". *WGN, Journal of the IMO*, **47:3**, 79–92.

Smirnov V. A. (2015). "About the nature of meteor flares". *Odessa Astronomical Publications*, **28**, 58.

Stenbaek-Nielsen H. C. and Jenniskens P. (March 2003). "Leonid at 1000 frames per second". In *The Institute of Space and Astronautical Science Report SP No. 15*.

Vinković D. and Grisevich M. (2020). "The challenges in hypervelocity microphysics research on meteoroid impacts into the atmosphere". *Journal of the Geographical Institute "Jovan Cvijic", SASA*, **70:1**, 45–55.

Handling Editor: Željko Andreić

Spectroscopy during the Perseids shower maximum 2022

Bill Ward[1]

A high-resolution spectrum captured during the Perseid 2022 shower is analysed. Two additional fireballs were captured and the difference in their spectra is examined.

Received 2022 October 12

1 Introduction

A test using a transmission grating with 830 grooves per mm fitted to a ZWO 174MM camera/25 mm $f/1.3$ lens system was carried out during the Perseid 2022 maximum. Several bright fireball spectra were captured but, as is common with meteor spectroscopy due to the random fall of any meteor, most of these were only small sections of the spectrum. One spectrum, however, was captured that spanned most of the visible wavelength range. That is discussed here.

2 High Resolution Spectrum Image

A significant advantage of the ZWO 174MM camera is the global shutter. This means each video frame is a complete image of the whole field of view. This allows for easier image processing and greatly improves the overall quality of the images.

Figure 1 shows the raw composite video image of the fireball spectrum on 2022 August 14 at $00^{h}32^{m}58^{s}$ UT. Figure 2 shows a crop of the spectrum that has been further processed and the many lines present. The IRIS image processing package was used for this.[a]

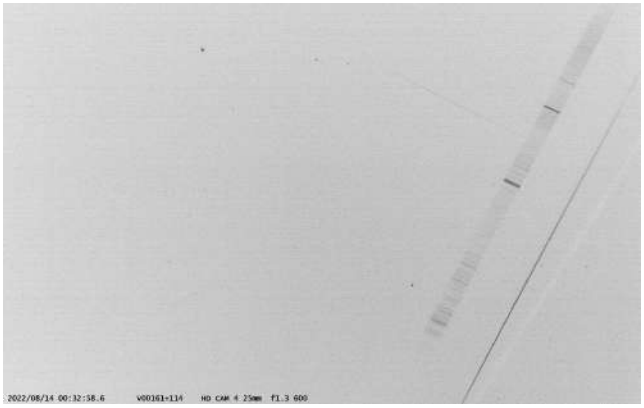

Figure 1 – Raw image of Perseid fireball spectrum. Negative image is shown here for better reproduction.

The first task is to wavelength calibrate the image. This is done using Visual Spec.[b] The brightest lines are assumed to be known by comparison with other spectra and laboratory lists of element emissions (Ward, 2015).

Once the major lines, for example sodium and magnesium, have been established, the weaker lines can then be "fitted" by comparing the measured wavelengths to the reference emission data.

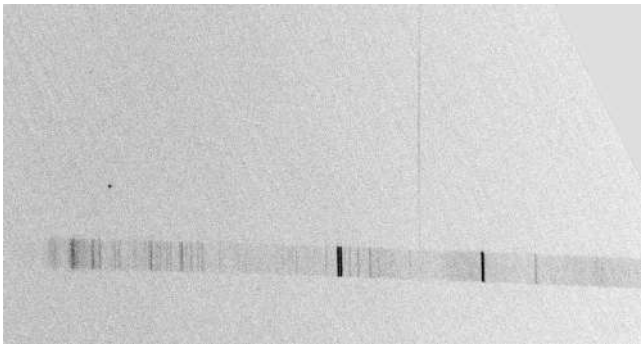

Figure 2 – Crop and reprocessed image of Perseid fireball spectrum. Negative image is shown here for better reproduction.

To correct for instrument response the spectrum is now divided through, by a known flux standard. Using the library supplied with the Visual Spec software, Vega was used. The wavelength calibrated and instrument response corrected spectrum plot is shown in Figure 3. A colourised synthetic spectrum is shown in Figure 4.

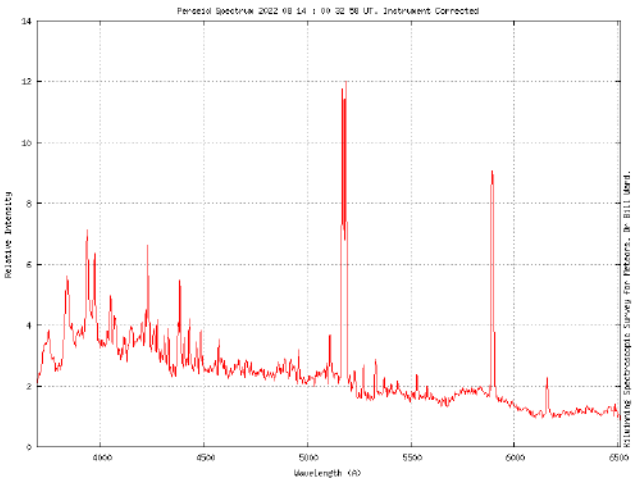

Figure 3 – Spectrum plot of Perseid fireball.

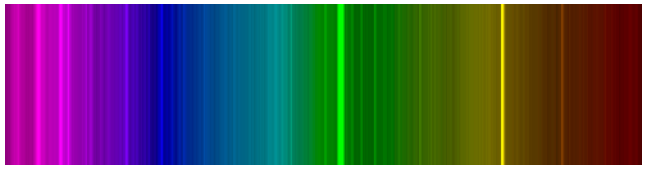

Figure 4 – Colourised synthetic spectrum.

Examining the spectrum reveals that the strongest emission is from neutral magnesium (triplet) at 517 nm. This triplet is partially resolved in the spectrum image.

[1]UWS, Tom Howie Building, High Street, Paisley, PA1 2BE. Email: bill_meteor@yahoo.com

IMO bibcode WGN-506-ward-spectroscopy
NASA-ADS bibcode 2022JIMO...50..179W

[a] http://www.astrosurf.com/buil/iris-software.html
[b] http://astrosurf.com/vdesnoux/

Next strongest is the sodium doublet at 589 nm. This spectrum is of a cometary refractory material and has the typical appearance as recorded in previous years, Figure 5.

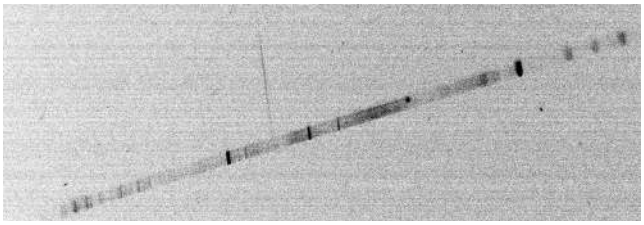

Figure 5 – Perseid fireball spectrum from 2020. 600 grooves/mm transmission grating used. Negative image is shown here for better reproduction.

3 Other Perseid spectrum comparison

A bright fireball was observed visually on 2022 August 10 at $02^{h}11^{m}16^{s}$ UT Initially it was thought to be a Perseid given its path. The fireball was also captured by both a WATEC 910 camera fitted with a Computar 2.8 mm $f/1.0$ lens, Figure 6 and another WATEC 910 camera fitted with a 12 mm $f/0.8$ Lens and 600 grooves/mm transmission grating, Figure 7.

Figure 6 – Suspected Perseid fireball, 2022 August 10 at $02^{h}11^{m}16^{s}$ UT.

This spectrum is well dispersed and detailed. However closer examination of the images reveal some interesting features. Visually it was assigned as a Perseid but the wide field view shows the fireball is not quite aligned to the radiant. Also examining the spectrum it can be seen that there is no emission from the forbidden oxygen transition at 557.7 nm.

This was noticeable as all previous Perseids spectra are seen to have this distinctive emission due to their high geocentric velocity of 61 km/s (Kronk, 2014). By lacking this line it indicates that the meteor was not travelling as fast as a normal Perseid. This emission only occurs in high speed meteors that start to ablate above ~ 110 km. Here the atmospheric conditions are such that the electrons are not robbed of energy through collisional de-excitation allowing the transition at 557.7 nm to occur (McKinley, 1961).

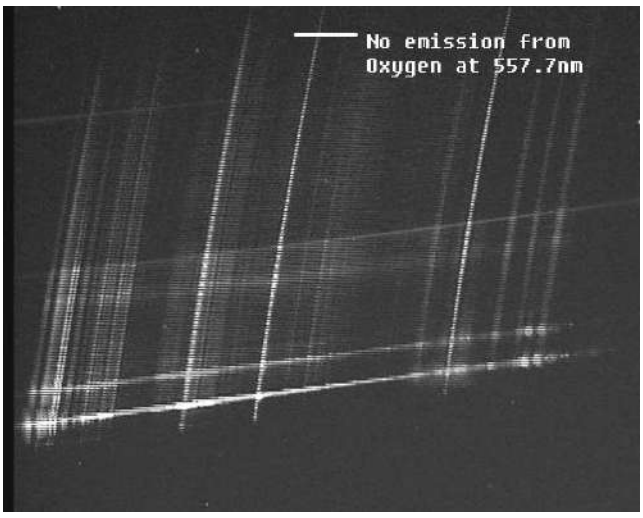

Figure 7 – Spectrum of suspected Perseid fireball.

By good fortune another fireball was captured by the same camera systems the following night at 2022 August 11 at $01^{h}53^{m}18^{s}$ UT. The wide field and spectrum images are shown in Figures 8 and 9. Inspection of the spectrum images reveals the characteristic emission of the 557.7 nm line indicating that this was a fast meteor consistent with the Perseids.

Figure 8 – Perseid fireball, 2022 August 11 at $01^{h}53^{m}18^{s}$ UT.

Communication with Alex Pratt of the NEMETODE group confirmed that the first fireball was indeed a lower velocity sporadic fireball. Its appearance near to Perseid radiant was a chance alignment.

4 Conclusions and future plans

The test of the 830 grooves/mm transmission grating has proven successful with the capture of an extremely well resolved spectrum of a Perseid fireball. There is always the compromise that as the groove count and the dispersion both increase, the number of available spectra falls. This is due to the greater dispersion requiring a brighter meteor to give a viable spectrum, all other things being equal. Also, as the spectrum is geometrically longer, less is likely to be seen in the field of view.

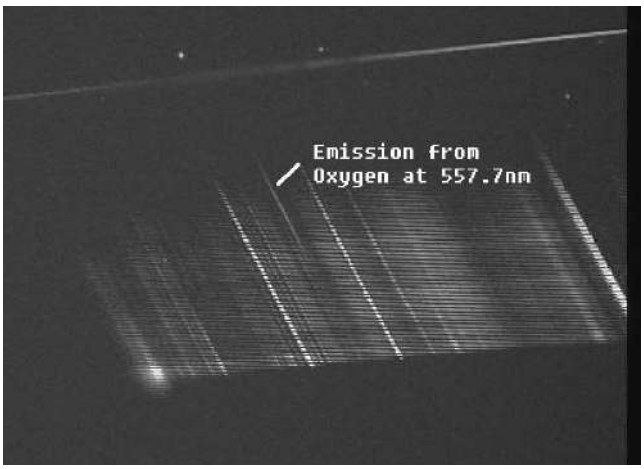

Figure 9 – Spectrum of Perseid fireball showing forbidden Oxigen emission at 557.7 nm.

Even without a full wavelength analysis, a spectrum can reveal "secondary" information about the meteor. This is illustrated by the example whereby the absence of the 557.7 nm line immediately indicates a velocity limit approximation. In this case it indicated that the fireball may not have been a Perseid as was initially thought. Without access to the spectrum information, or indeed the video imaging, a visual observer may incorrectly have assigned this fireball as another Perseid.

The Kilwinning Spectroscopic Survey for Meteors has been taking meteor spectra for over a decade. Until this test, 600 grooves/mm gratings have been used. As a result of this test a second 830 grooves/mm transmission grating will be installed on another ZWO 174MM plus 25 mm $f/1.3$ system in the near future.

Acknowledgments

Thanks to Alex Pratt for co-ordinating the observations from other NEMETODE observers and confirming the non-Perseid nature of the fireball on 2022 August 10.

References

Kronk G. W. (2014). *Meteor Showers, An Annotated Catalogue*. Springer, 188 ff pages.

McKinley D. W. R. (1961). *Meteor Science and Engineering*. McGraw Hill Publishing, 143 ff pages.

Ward B. (2015). "Spectroscopy of the Quadrantids". *WGN, Journal of the IMO*, **43:4**, 102–105.

Handling Editor: Javor Kac

The International Meteor Organization

www.imo.net

Follow us on Facebook InternationalMeteorOrganization

Follow us on Twitter @IMOMeteors

Council

President: Cis Verbeeck,
Bogaertsheide 5, 2560 Kessel, Belgium.
e-mail: cis.verbeeck@gmail.com

Vice-President: Juraj Tóth,
Fac. Math., Phys. & Inf., Comenius Univ.,
Mlynska dolina, 84248 Bratislava, Slovakia.
e-mail: toth@fmph.uniba.sk

Secretary-General: Robert Lunsford,
14884 Quail Valley Way, El Cajon,
CA 92021-2227, USA. tel. +1 619 755 7791
e-mail: lunro.imo.usa@cox.net

Treasurer: Marc Gyssens, Heerbaan 74,
B-2530 Boechout, Belgium.
e-mail: marc.gyssens@uhasselt.be
BIC: GEBABEBB
IBAN: BE30 0014 7327 5911
Bank transfer costs are always at your expense.

Other Council members:
Karl Antier, 16, rue de la République,
F-04100 Manosque, France.
e-mail: karl.antier@gmx.fr
Javor Kac (see details under WGN)
Detlef Koschny, Zeestraat 46,
NL-2211 XH Noordwijkerhout, Netherlands.
e-mail: detlef.koschny@tum.de
Sirko Molau, Abenstalstraße 13b, D-84072
Seysdorf, Germany. e-mail: sirko@molau.de
Francisco Ocaña Gonzalez, C/ Arquitectura, 7.
28005 Madrid, Spain.
e-mail: francisco.ocana.gonzalez@gmail.com
Vincent Perlerin, 16, rue Georges Bernanos,
51100 Reims, France.
e-mail: vperlerin@gmail.com
Jürgen Rendtel, Eschenweg 16, D-14476
Marquardt, Germany. e-mail: jrendtel@aip.de

Commission Directors

Visual Commission: Jürgen Rendtel
Generic e-mail address: visual@imo.net
Electronic visual report form:
http://www.imo.net/visual/report/electronic
Video Commission: Sirko Molau (video@imo.net)
Photographic Commission: Bill Ward
(bill_meteor@yahoo.com)
Generic e-mail address: photo@imo.net
Radio Commission: Chris Steyaert
(radio@imo.net)
Fireballs: Online fireball reports:
http://fireballs.imo.net

Webmaster

Karl Antier, e-mail: webmaster@imo.net

WGN

Editor-in-chief: Javor Kac
Na Ajdov hrib 24, SI-2310 Slovenska Bistrica,
Slovenia. e-mail: wgn@imo.net;
include METEOR in the e-mail subject line

Editorial board: Ž. Andreić, D.J. Asher,
F. Bettonvil, M. Gyssens, C. Hergenrother,
T. Heywood, J. Rendtel, C. Verbeeck,
S. de Vet, D. Vida.

IMO Sales

Available from the Treasurer or the Electronic Shop on the IMO Website	€	$
IMO membership, including subscription to WGN Vol. 50 (2022)		
Surface mail	26	32
Air Mail (outside Europe only)	49	60
Electronic subscription only	21	25
Proceedings of the International Meteor Conference on paper		
1990, 1991, 1995, 1996, 1999, 2000, 2002, 2003, per year	9	12
2007, 2010, 2011, per year	15	20
2012, 2013, 2015, 2017 per year	25	32
Proceedings of the Meteor Orbit Determination Workshop 2006	15	20
Radio Meteor School Proceedings 2005	15	20
Handbook for Meteor Observers	23	29
Meteor Shower Workbook	12	16
Electronic media		
Meteor Beliefs Project ZIP archive	6	8

2022 Tau Herculids from Arizona

Composite image of about 100 meteors captured during the Tau Herculid campaign on 2022 May 31 from $03^{\mathrm{h}}42^{\mathrm{m}}$ to $11^{\mathrm{h}}02^{\mathrm{m}}$ UT from Double R Ranch, Arizona, USA. ZWO ASI 294MC Pro camera was used with Sigma 28-mm $f/1.4$ lens and $\frac{1}{2}$ s exposure.

The field covers 66° in azimuth and 63° in elevation. Image courtesy: Ján Mäsiar.